ARTICLE

Humoral immunity to SARS-CoV-2 elicited by combination COVID-19 vaccination regimens

Zijun Wang[1]*, Frauke Muecksch[2]*, Friederike Muenn[3]*, Alice Cho[1]*, Shuai Zong[1], Raphael Raspe[1], Victor Ramos[1], Brianna Johnson[1], Tarek Ben Tanfous[1], Justin DaSilva[2], Eva Bednarski[2], Camila Guzman-Cardozo[2], Martina Turroja[1], Katrina G. Millard[1], Pinkus Tober-Lau[3], David Hillus[3], Kai-Hui Yao[1], Irina Shimeliovich[1], Juan Dizon[1], Anna Kaczynska[1], Mila Jankovic[1], Anna Gazumyan[1], Thiago Y. Oliveira[1], Marina Caskey[1], Paul D. Bieniasz[2,4], Theodora Hatziioannou[2], Florian Kurth[3], Leif Erik Sander[3,5], Michel C. Nussenzweig[1,4], and Christian Gaebler[1,3]

The SARS-CoV-2 pandemic prompted a global vaccination effort and the development of numerous COVID-19 vaccines at an unprecedented scale and pace. As a result, current COVID-19 vaccination regimens comprise diverse vaccine modalities, immunogen combinations, and dosing intervals. Here, we compare vaccine-specific antibody and memory B cell responses following two-dose mRNA, single-dose Ad26.COV.2S, and two-dose ChAdOx1, or combination ChAdOx1/mRNA vaccination. Plasma-neutralizing activity, as well as the magnitude, clonal composition, and antibody maturation of the RBD-specific memory B cell compartments, showed substantial differences between the vaccination regimens. While individual monoclonal antibodies derived from memory B cells exhibited similar binding affinities and neutralizing potency against Wuhan-Hu-1 SARS-CoV-2, there were significant differences in epitope specificity and neutralizing breadth against viral variants of concern. Although the ChAdOx1 vaccine was inferior to mRNA and Ad26.COV.2S in several respects, biochemical and structural analyses revealed enrichment in a subgroup of memory B cell neutralizing antibodies with distinct RBD-binding properties resulting in remarkable potency and breadth.

Introduction

Coronavirus disease 2019 (COVID-19) vaccine programs are a historic public health success that saved countless lives and prevented millions of severe acute respiratory syndrome coronavirus (SARS-CoV-2) infections (Vilches et al., 2022). Vaccination is a multifaceted global effort involving a diverse collection of vaccine platforms including mRNA, adenoviral vector–based, inactivated virus, and recombinant protein immunogens (Mathieu et al., 2021). A detailed evaluation of the different vaccine-specific immune responses will inform improved vaccination strategies for the prevention of COVID-19 and other respiratory viral infections of pandemic potential (Zhang et al., 2022).

With close to 2.5 billion administered doses, the ChAdOx1 nCoV-19 (AZD1222) vaccine accounted for over one third of all global COVID-19 vaccine doses administered in 2021 (Mallapaty et al., 2021; Mathieu et al., 2021). The ChAdOx1 vaccine encodes full-length WT (Wuhan-Hu-1) SARS-CoV-2 spike protein without the prefusion-stabilizing mutations found in the three US-approved vaccines (BNT162b2, mRNA-1273, and Ad26.COV.2S;

Watanabe et al., 2021). Outside of the US, ChAdOx1 received regulatory approval as a two-dose vaccine administered at an interval of 4–12 wk. Unfortunately, ChAdOx1 vaccination was associated with immune thrombocytopenia, a rare but serious complication that has been described after the administration of adenoviral vector vaccines. As a result, many individuals receiving a ChAdOx1 prime were subsequently boosted with an mRNA vaccine (Klok et al., 2022).

The combination (ChAdOx1/mRNA vaccine) prime-boost regimen showed enhanced immunogenicity (Barros-Martins et al., 2021; Hillus et al., 2021; Normark et al., 2021; Schmidt et al., 2021); however both the ChadOx1-based vaccine regimens proved to be effective with substantial protection against COVID-19 hospitalization and death (Andrews et al., 2022; Nordstrom et al., 2021).

In-depth analyses of antibody and memory B cell responses after natural infection and mRNA (BNT162b2, mRNA-1273) and Ad26.COV.2S vaccination have been performed (Cho et al., 2021; Gaebler et al., 2021; Muecksch et al., 2022; Robbiani et al., 2020;

[1]Laboratory of Molecular Immunology, The Rockefeller University, New York, NY;   [2]Laboratory of Retrovirology, The Rockefeller University, New York, NY;   [3]Department of Infectious Diseases and Respiratory Medicine, Charité–Universitätsmedizin Berlin, Berlin, Germany;   [4]Howard Hughes Medical Institute, The Rockefeller University, New York, NY;   [5]Berlin Institute of Health (BIH), Berlin, Germany.

*Z. Wang, F. Muecksch, F. Muenn, and A. Cho contributed equally to this paper.   Correspondence to Christian Gaebler: cgaebler01@rockefeller.edu;   Michel C. Nussenzweig: nussen@rockefeller.edu.

Wang et al., 2021c; Wang et al., 2021d). However, far less is known about the responses elicited by the ChadOx1 vaccine, even though it was used in more countries than any other COVID-19 vaccine (Mathieu et al., 2021). Here, we compare vaccine-specific antibody and memory B cell responses to two-dose mRNA (BNT162b2 or mRNA-1273), one-dose Ad26.COV.2S, two-dose ChAdOx1 (AZ/AZ), or ChAdOx1/BNT162b2 combination (AZ/BNT) vaccines.

Results

Four cohorts of study participants with different vaccination regimens were recruited and sampled prospectively. All cohorts included sampling time points at ∼1 and 6 mo after the first vaccine dose. An additional sampling time point at 1 mo after second vaccination was available for the mRNA (1.3 mo after the second dose = 2.3 mo after first dose), AZ/BNT, and AZ/AZ (1 mo after second dose = 4 mo after first dose) two-dose vaccination regimens. Sampling at 1 mo after the first AZ dose allowed for longitudinal or cross-sectional comparisons within the AZ/BNT or AZ/AZ cohort, respectively. The vaccination and blood collection schedule for all cohorts in this study is depicted in Fig. 1 A. For the AZ/BNT and AZ/AZ cohort, a total of 49 healthcare workers with no prior history of SARS-CoV-2 infection who received a ChAdOx1 vaccine prime followed by ChAdOx1 or BNT162b2 boost 10–12-wk later were enrolled in a prospective observational cohort study in Berlin, Germany (Hillus et al., 2021). A total of 23 and 26 study participants received ChAdOx1 or mRNA as a second dose, respectively. Volunteers ranged in age from 20 to 65 yr and were 65% female (AZ/AZ average age 48.8, age range 23–65; AZ/BNT average age 40.6, age range 20–65). The demographic characteristics and intervals between vaccine doses and blood collections are comparable between AZ/AZ and AZ/BNT participants (Fig. S1, Q–V). Participants in the AZ/AZ cohort were moderately older than participants in the mRNA cohort (average age AZ/AZ 48.8 yr vs. mRNA 37.5 yr, P = 0.0091); all other cohorts were comparable for age and sex (Fig. S1, Q and R). For detailed demographic information, see Materials and methods, Fig. S1, Q–V, Table S1, and Cho et al. (2022), Muecksch et al. (2022).

Plasma binding and neutralization

Plasma antibody binding titers to SARS-CoV-2 receptor-binding domain (RBD) were measured by ELISAs (Cho et al., 2021; Wang et al., 2021c). RBD-binding IgG levels 1 mo after ChAdOx1 prime were lower but not significantly different from antibody levels following a single dose of an mRNA vaccine (Cho et al., 2021) or the Ad26.COV.2S vaccine (Cho et al., 2022) at similar time points (Fig. 1, B and C). ChAdOx1 and mRNA boosting enhanced IgG titers 12-fold (AZ/BNT) and 2.6-fold (AZ/AZ) 1 mo after the second vaccine dose, respectively (P < 0.0001; Fig. 1, B and D). In both cases, anti-RBD antibodies in plasma decreased significantly between 4 and 6 mo (AZ/BNT: 3.2-fold, P < 0.0001; AZ/AZ: 1.5-fold, P = 0.0022; Fig. 1 B), but antibodies binding to RBD following combination AZ/BNT vaccination remained significantly higher 6 mo after the initial priming dose (P < 0.0001, Fig. 1 B). Anti-RBD IgG levels after the AZ/BNT boost were

directly correlated with initial antibody levels after the prime (Fig. S1 A; r = 0.50, P = 0.012). Consistent with other reports (Barros-Martins et al., 2021; Kaku et al., 2022; Pozzetto et al., 2021), AZ/BNT vaccinees exhibited anti-RBD plasma reactivity 6 mo after the initial prime, which was comparable to individuals who received two doses of an mRNA vaccine. Both AZ/BNT and mRNA vaccinees showed significantly higher serum antibody levels than individuals who received one dose of the Ad26.-COV.2S vaccine (Fig. 1, D and E). By contrast and in line with other studies (GeurtsvanKessel et al., 2022; Muecksch et al., 2022), antibody levels following AZ/AZ vaccination remained lower compared to individuals who received two doses of an mRNA vaccine, but the difference did not reach statistical significance (P = 0.12; Fig. 1 E). In addition, individuals who received AZ/AZ vaccination showed serum antibody levels that were slightly but not significantly higher than those of Ad26.COV.2S vaccinees 6 mo after vaccination (P = 0.075; Fig. 1 E). In contrast to IgG, AZ/BNT and AZ/AZ vaccination induced similar IgM and IgA anti-RBD antibody levels (Fig. S1, B and C).

RBD-binding IgG titers were negatively correlated with age 4 mo after the initial prime for AZ/AZ. No inverse correlation between age and RBD-binding antibodies was observed 6 mo after the initial prime or after AZ/BNT vaccination (r = −0.51, P = 0.015; Fig. S1, D and E). In addition, there were no sex-related differences in antibody levels following AZ/BNT or AZ/AZ vaccination (Fig. S1 F). Notably, 4 mo after the initial prime, antibody levels in AZ/BNT vaccinees were negatively correlated with the interval between prime and second vaccination, suggesting that earlier administration of a heterologous booster vaccination may result in optimal protection (r = −0.50, P = 0.010; Fig. S1, G and H).

Neutralizing activity was determined for the same participants using HIV-1 pseudotyped with Wuhan-Hu-1 SARS-CoV-2 spike (S) protein (Robbiani et al., 2020; Schmidt et al., 2020; Table S1). The geometric mean half-maximal neutralizing titer (NT_{50}) 1 mo after the ChAdOx1 initial prime was comparable to a single dose of an mRNA vaccine (Cho et al., 2021) or Ad26.COV.2S (Cho et al., 2022) vaccine (Fig. 1, F and G). Administration of a second dose increased NT_{50}s among AZ/BNT and AZ/AZ vaccinees from 139 to 1,946 and 305, respectively (P < 0.0001; Fig. 1 F). In line with the greater initial neutralizing activity, the decrease between 4 and 6 mo after the initial prime was more pronounced among combination AZ/BNT than AZ/AZ vaccinees (4.6-fold, P < 0.0001 vs. 1.8-fold, P = 0.0066 respectively; Fig. 1 F). Nevertheless, compared to AZ/AZ vaccinees, plasma-neutralizing activity remained significantly higher 6 mo after the initial prime in AZ/BNT vaccinees (P = 0.01; Fig. 1 F).

Consistent with ELISA reactivity, AZ/BNT elicited similar neutralizing activity as two doses of an mRNA vaccine 6 mo after the initial prime. In addition, both AZ/BNT and mRNA vaccinees showed significantly higher serum antibody levels than individuals who received one dose of the Ad26.COV.2S vaccine (Fig. 1 I). By contrast, plasma-neutralizing activity after AZ/AZ vaccination was substantially lower than in individuals who received two doses of an mRNA vaccine, but exceeded neutralizing titers of individuals that received a single dose of the Ad26.COV.2S vaccine (Fig. 1, H and I).
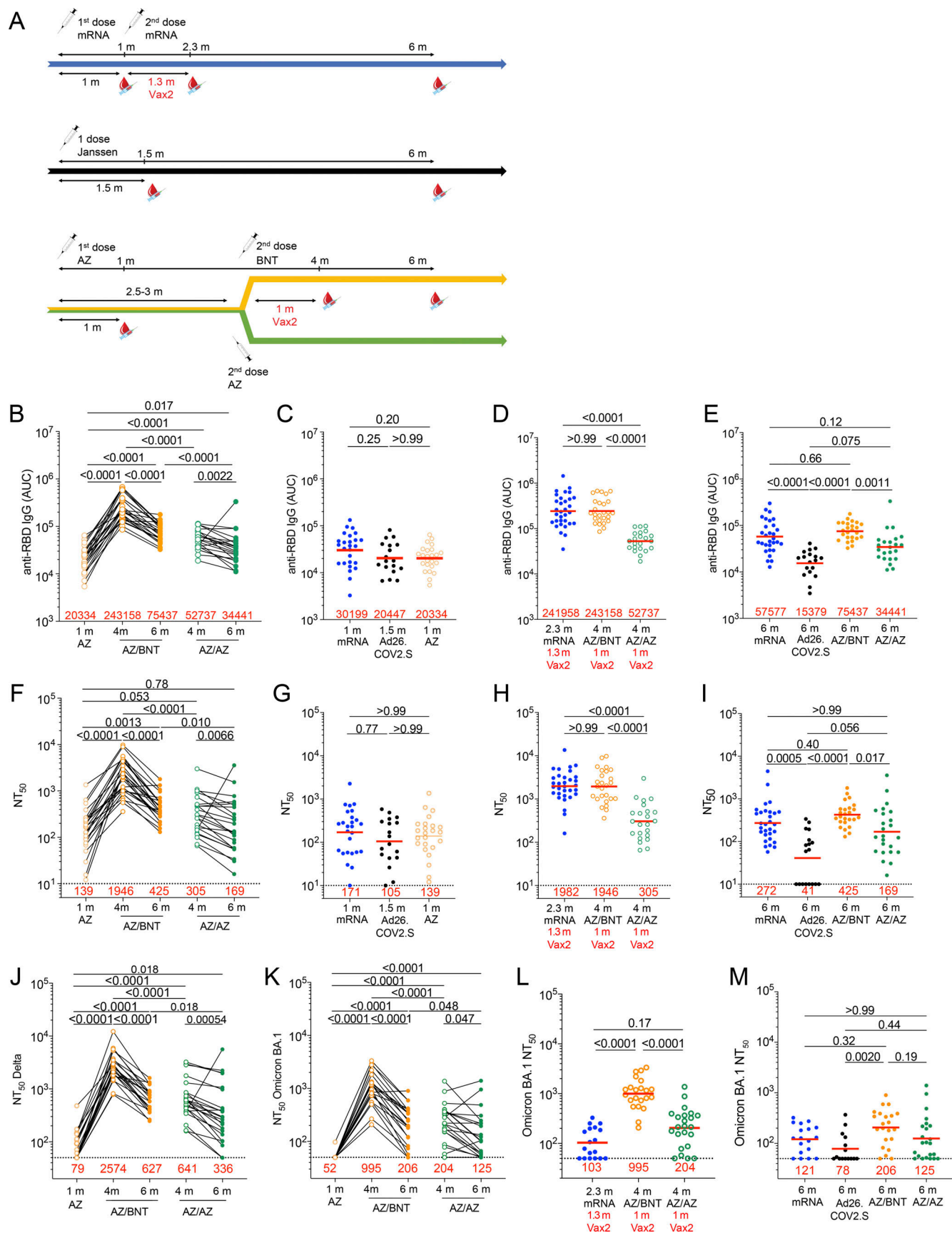
Wang et al.
In-depth immunological COVID-19 vaccine comparison

Journal of Experimental Medicine 2 of 15
https://doi.org/10.1084/jem.20220826

A

1st dose mRNA   2nd dose mRNA

1 m   2.3 m   6 m

1 m   1.3 m Vax2

1 dose Janssen   1.5 m   6 m

1.5 m

1st dose AZ   1 m   2nd dose BNT   4 m   6 m

2.5–3 m

1 m   1 m Vax2

2nd dose AZ

B
anti-RBD IgG (AUC)

0.017
<0.0001
<0.0001
<0.0001   <0.0001
<0.0001 <0.0001   0.0022

20334   243158   75437   52737   34441
1 m AZ   4 m   6 m   4 m   6 m
AZ/BNT   AZ/AZ

C
anti-RBD IgG (AUC)

0.20
0.25   >0.99

30199   20447   20334
1 m mRNA   1.5 m Ad26.COV2.S   1 m AZ

D
anti-RBD IgG (AUC)

<0.0001
>0.99   <0.0001

241958   243158   52737
2.3 m mRNA   4 m AZ/BNT   6 m AZ/AZ
1.3 m Vax2   1 m Vax2   1 m Vax2

E
anti-RBD IgG (AUC)

0.12
0.075
0.66
<0.0001 <0.0001   0.0011

57577   15379   75437   34441
6 m mRNA   6 m Ad26.COV2.S   6 m AZ/BNT   6 m AZ/AZ

F
NT_{50}

0.78
0.053
<0.0001
0.0013   0.010
<0.0001 <0.0001   0.0066

139   1946   425   305   169
1 m AZ   4 m   6 m   4 m   6 m
AZ/BNT   AZ/AZ

G
NT_{50}

>0.99
0.77   >0.99

171   105   139
1 m mRNA   1.5 m Ad26.COV2.S   1 m AZ

H
NT_{50}

<0.0001
>0.99   <0.0001

1982   1946   305
2.3 m mRNA   4 m AZ/BNT   6 m AZ/AZ
1.3 m Vax2   1 m Vax2   1 m Vax2

I
NT_{50}

>0.99
0.056
0.40
0.0005   <0.0001   0.017

272   41   425   169
6 m mRNA   6 m Ad26.COV2.S   6 m AZ/BNT   6 m AZ/AZ

J
NT_{50} Delta

0.018
<0.0001
<0.0001
<0.0001   0.018
<0.0001 <0.0001   0.00054

79   2574   627   641   336
1 m AZ   4 m   6 m   4 m   6 m
AZ/BNT   AZ/AZ

K
NT_{50} Omicron BA.1

<0.0001
<0.0001
<0.0001
<0.0001   0.048
<0.0001 <0.0001   0.047

52   995   206   204   125
1 m AZ   4 m   6 m   4 m   6 m
AZ/BNT   AZ/AZ

L
Omicron BA.1 NT_{50}

0.17
<0.0001   <0.0001

103   995   204
2.3 m mRNA   4 m AZ/BNT   6 m AZ/AZ
1.3 m Vax2   1 m Vax2   1 m Vax2

M
Omicron BA.1 NT_{50}

>0.99
0.44
0.32
0.0020   0.19

121   78   206   125
6 m mRNA   6 m Ad26.COV2.S   6 m AZ/BNT   6 m AZ/AZ

Figure 1. **Plasma binding and neutralizing activity. (A)** Vaccination and blood donation schedules for mRNA vaccinees (upper panel), Ad26.COV2.S vaccinees (middle panel), and ChAdOx1 (AZ) vaccinees boosted with either BNT162b2 (BNT, upper half of lower panel) or AZ (lower half of lower panel).

(B) AUC for plasma IgG antibody binding to SARS-CoV-2 Wuhan-Hu-1 RBD 1 mo (m) after mRNA prime (Cho et al., 2021), or Ad26.COV.2S prime (Cho et al., 2022) or AZ prime, as well as 4 mo or 6 mo after the initial AZ prime (AZ/BNT, n = 26; or AZ/AZ, n = 23). Lines connect longitudinal samples. **(C–E)** AUC for plasma IgG binding to Wuhan-Hu-1 RBD in vaccinees 1 mo after AZ prime compared to mRNA prime (Cho et al., 2021) or Ad26.COV.2S (Cho et al., 2022) prime at similar timepoint (C), mRNA vaccinees 2.3 mo after initial dose (Cho et al., 2021) compared to AZ/BNT and AZ/AZ vaccinees 4 mo after initial dose (D), or mRNA vaccinees 6 mo after initial dose (Cho et al., 2021) and Ad26.COV.2S vaccinees 6 mo after one dose (Cho et al., 2022) compared to AZ/BNT and AZ/AZ vaccinees 6 mo after initial dose (E). **(F–I)** Anti–SARS-CoV-2 NT$_{50}$s of plasma measured by a SARS-CoV-2 pseudotype virus neutralization assay using WT (Wuhan-Hu-1; Wu et al., 2020) SARS-CoV-2 pseudovirus (Robbiani et al., 2020; Schmidt et al., 2020) in plasma samples shown in A–E. **(J–M)** Plasma-neutralizing activity against indicated SARS-CoV-2 Delta (J) and Omicron (K) variants for n = 45 (AZ/BNT, n = 22; and AZ/AZ, n = 23) randomly selected samples assayed in HT1080Ace2 cl.14 cells. **(L and M)** mRNA vaccinees 2.3 mo after initial dose (Cho et al., 2021) compared to AZ/BNT and AZ/AZ vaccinees 4 mo after initial dose (L), or mRNA vaccinees 6 mo (Cho et al., 2021) and Ad26.COV.2S vaccinees 6 mo after initial dose (Cho et al., 2022) compared to AZ/BNT and AZ/AZ vaccinees 6 mo after initial dose (M). See Materials and methods for a list of all substitutions/deletions/insertions in the spike variants. Deletions/substitutions corresponding to viral variants were incorporated into a spike protein that also includes the R683G substitution, which disrupts the furin cleavage site and increases particle infectivity. All experiments were performed at least in duplicate. Red bars and values represent geometric mean values. Statistical significance was determined by two-tailed Mann-Whitney test for unpaired observations or by Wilcoxon matched-pairs signed rank test for paired observations followed by Holm-Šídák test for multiple comparisons, longitudinal comparisons within the same cohort (AZ/BNT: AZ 1 mo vs. AZ/BNT 4 mo vs. AZ/BNT 6 mo; or AZ/AZ: AZ/AZ 4 mo vs. AZ/AZ 6 mo) were analyzed using Wilcoxon matched-pairs signed rank test; all other comparisons (e.g., those across different cohorts) were analyzed using two-tailed Mann-Whitney statistical tests. All resulting P values for each figure were corrected for multiple comparisons by Holm-Šídák test (B, F, and J–K), or two-tailed Kruskal–Wallis test with subsequent Dunn's multiple comparisons (C–E, G–I, L, and M).

Plasma-neutralizing activity for 45 participants with sufficient sample availability (n = 22, AZ/BNT; n = 23, AZ/AZ) was also assessed against SARS-CoV-2 Delta and Omicron BA.1 variants using viruses pseudotyped with appropriate variant spikes (Cho et al., 2021; Schmidt et al., 2022; Schmidt et al., 2020; Wang et al., 2021d). 4 mo after the initial AZ/BNT prime vaccination, neutralizing titers against Delta and Omicron BA.1 were 5.7- and 14.7-fold lower than against Wuhan-Hu-1, with a further decrease to 5.7- and 17.3-fold lower activity at the 6-mo time point respectively (Fig. 1, J and K; and Fig. S1 I). Similarly, AZ/AZ vaccination resulted in 5.7- and 17.9-fold lower neutralizing activity against Delta and Omicron BA.1 than against Wuhan-Hu-1 respectively at the 4-mo time point. While Delta neutralization further decreased 5.9-fold compared to Wuhan-Hu-1 at the 6-mo time point, the neutralizing activity against Omicron BA.1, which was initially very low, decreased to a lesser extent among AZ/AZ vaccinees (Fig. 1, J and K; and Fig. S1, I–K).

Remarkably, 1 mo after the second vaccine dose, Omicron BA.1–neutralizing titers in combination with AZ/BNT vaccinees exceeded neutralizing activity after AZ/AZ or two-dose mRNA vaccination at similar time points by 4.9- and 9.7-fold, respectively (P < 0.0001 and P < 0.0001; Fig. 1 L). Omicron BA.1–neutralizing titers remained higher in AZ/BNT vaccinees but were not statistically different from mRNA or AZ/AZ vaccinees 6 mo after the prime, while titers in Ad26.COV.2S vaccinees were significantly lower (Fig. 1 M). The ratio of plasma-neutralizing titers against Delta:Wuhan-Hu-1 was significantly lower in individuals who received AZ/AZ or AZ/BNT as compared to those who received two doses of mRNA or one dose of Ad26.COV.2S. However, no major differences were found among different vaccination regimens regarding the neutralizing titers against Omicron BA.1:Wuhan-Hu-1 (Fig. S1 W).

Memory B cell responses to SARS-CoV-2 RBD and N-terminal domain (NTD)

To compare the development of B cell memory after COVID-19 vaccination, we initially enumerated memory B cells expressing surface receptors binding to the RBD and NTD of the SARS-CoV-2 spike protein using fluorescently labeled proteins (Fig. 2 A and Fig. S2, A–E). The frequency of RBD-binding memory B cells found in circulation 1 mo after AZ prime was significantly lower than after mRNA (P < 0.0001; Bednarski et al., 2022 Preprint; Cho et al., 2021) and Ad26.COV.2S vaccination (P = 0.0029; Cho et al., 2022; Fig. 2 B). Although the frequency increased after AZ/BNT or AZ/AZ boosting (Fig. S2 D), two-dose mRNA vaccination resulted in significantly higher frequencies of RBD-binding memory B cells compared to all other vaccination regimens (Ad26.COV.2S: P = 0.014; AZ/BNT: P = 0.011; AZ/AZ: P < 0.0001; Fig. 2 C). By contrast, the frequency of NTD-binding memory B cells remained unchanged after the second dose (Fig. S2, C, E, and F), was similar to two-dose mRNA, and significantly lower than in Ad26.COV.2S vaccinees 6 mo after vaccination (AZ/BNT: P = 0.0007; AZ/AZ: P = 0.0001; Fig. S2 F).

To examine the specificity and neutralizing activity of the antibodies produced by memory cells, we purified single Wuhan-Hu-1 RBD-specific B cells, sequenced their antibody genes, and produced the recombinant antibodies in vitro. 450 paired anti-RBD antibody sequences were obtained from 22 vaccinees (AZ/BNT, n = 10; AZ/AZ, n = 12) sampled 6 mo after the initial prime (Fig. 2 D; Fig. S2, G and H; Fig. S3 A; and Table S2). Clonally expanded RBD-specific B cells across the different vaccine regimens 6 mo after prime represented 23, 13, 22, and 16% of all memory cells from mRNA, Ad26.COV.2S, AZ/BNT, and AZ/AZ vaccinees, respectively (Fig. 2 D). Similar to mRNA and Ad26.COV.2S vaccinees, *VH3-30*, *VH1-46*, and *VH3-53* genes were overrepresented among AZ/BNT and AZ/AZ vaccinees (Fig. S3, B–D; Cho et al., 2021; Cho et al., 2022). There was no difference in the number of somatic mutations between AZ/BNT or AZ/AZ vaccinees, although both groups showed significantly lower accumulation of somatic mutations than mRNA or Ad26.COV.2S vaccinees assayed at similar timepoints (P < 0.0001; Fig. 2 E).

We conclude that there are substantial differences in the magnitude, clonal composition, and antibody maturation of the RBD-specific memory B cell compartment between the different vaccination regimens. However, homologous and combination booster vaccination after a ChAdOx1 prime is not significantly
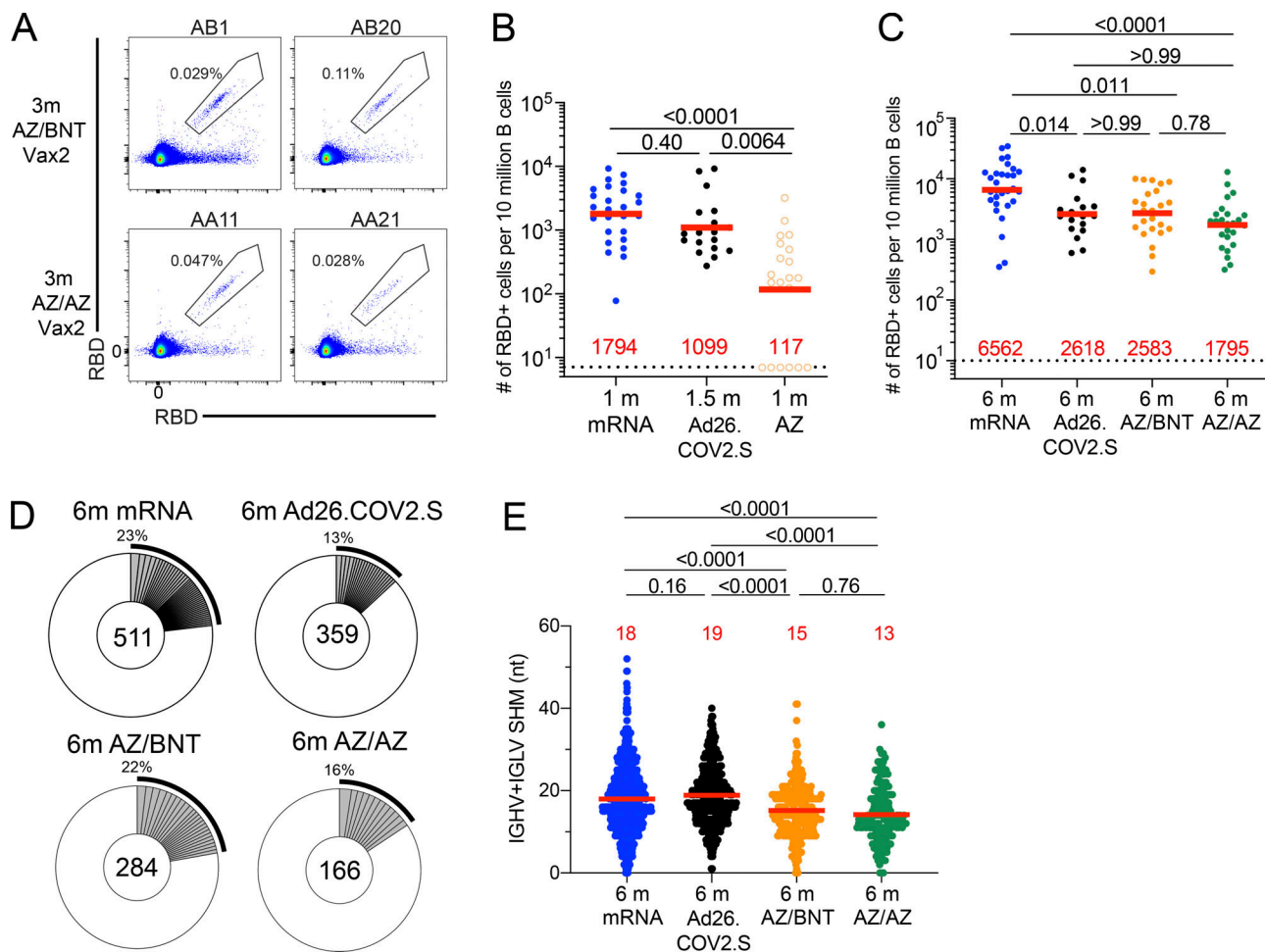
Figure 2. **Anti–SARS-CoV-2 RBD B cell memory. (A)** Representative flow cytometry plots showing dual AlexaFluor-647- and PE-Wuhan-Hu-1-RBD-binding single sorted B cells from ChAdOx1/BNT162b2 (AZ/BNT, n = 2) and ChAdOx1/ChAdOx1 (AZ/AZ, n = 2) vaccinees 6 mo (m) after initial dose. Gating strategy shown in Fig. S2. Percentage of antigen-specific B cells is indicated. **(B)** Frequency of Wuhan-Hu-1 RBD-specific B cells per 10 million (M) B cells in mRNA vaccinees 1 mo after prime (Cho et al., 2021) and Ad26.COV.2S vaccinees 1.5 mo after prime (Cho et al., 2022) compared to AZ vaccinees 1 mo after prime. **(C)** Frequency of Wuhan-Hu-1 RBD-specific B cells per 10 M B cells for mRNA vaccinees 6 mo after initial dose (Cho et al., 2021) and Ad26.COV.2S vaccinees 6 mo after prime (Cho et al., 2022) compared to AZ/BNT and AZ/AZ vaccinees 6 mo after initial dose. **(D)** Pie charts show the distribution of antibody sequences obtained from Wuhan-Hu-1 RBD-specific memory B cells of mRNA vaccinees 6 mo after initial dose and Ad26.COV.2S vaccinees 6 mo after initial prime, or AZ/BNT and AZ/AZ vaccinees 6 mo after initial dose. The number inside the circle indicates the aggregate number of sequences analyzed for each cohort. Gray slices indicate expanded clones (same *IGHV* and *IGLV* genes with highly similar CDR3s; see Materials and methods) found within the same individual. Pie slice size is proportional to the number of clonally related sequences. The black outline and associated numbers indicate the total percentage of clonally expanded sequences. **(E)** Number of nucleotide somatic hypermutations in *IGHV* + *IGLV* sequences obtained from Wuhan-Hu-1 RBD-specific memory B cells of mRNA vaccinees 6 mo after initial dose and Ad26.COV.2S vaccinees 6 mo after prime compared to AZ/BNT and AZ/AZ vaccinees 6 mo after initial dose. Red bars and numbers in B and C represent geometric mean value, and in E represent mean values. Statistical difference in B, C, and E was determined by two-tailed Kruskal–Wallis test with subsequent Dunn's multiple comparisons. All experiments were performed at least in duplicate.

different with respect to the frequency of memory B cells that develop or their levels of somatic mutation.

Neutralizing activity of mAbs

Next, we compared the neutralizing activity of mAbs elicited by mRNA, Ad26.COV.2S, and AZ/BNT or AZ/AZ vaccination. 291 anti-RBD mAbs were expressed and tested for binding by ELISA. 94% (n = 277) bound to the Wuhan-Hu-1 RBD, indicating the high efficiency of RBD-specific memory B cell isolation (Table S3). The geometric mean ELISA half-maximal concentration (EC_{50}) of the RBD-binding mAbs elicited by AZ/AZ or AZ/BNT vaccination was comparable (Fig. 3 A). EC_{50}s represent

an indirect measure of affinity. To directly examine anti-RBD antibody affinity, we performed biolayer interferometry (BLI) experiments on a subset of antibodies (n = 66 from AZ/BNT and n = 62 from AZ/AZ). Affinity was comparable among antibodies elicited by mRNA, Ad26.COV.2S, and AZ/BNT or AZ/AZ vaccination (Fig. 3 B; Cho et al., 2021). All 277 RBD-binding IgG mAbs were tested for neutralization against viruses pseudotyped with Wuhan-Hu-1 SARS-CoV-2 spike protein (183 and 94 antibodies isolated from AZ/BNT and AZ/AZ vaccinees, respectively). Memory B cell antibodies elicited by mRNA, Ad26.COV.2S, AZ/ BNT, and AZ/AZ vaccination 6 mo after the prime showed comparable activity (Fig. 3 C). Similarly, the proportion of
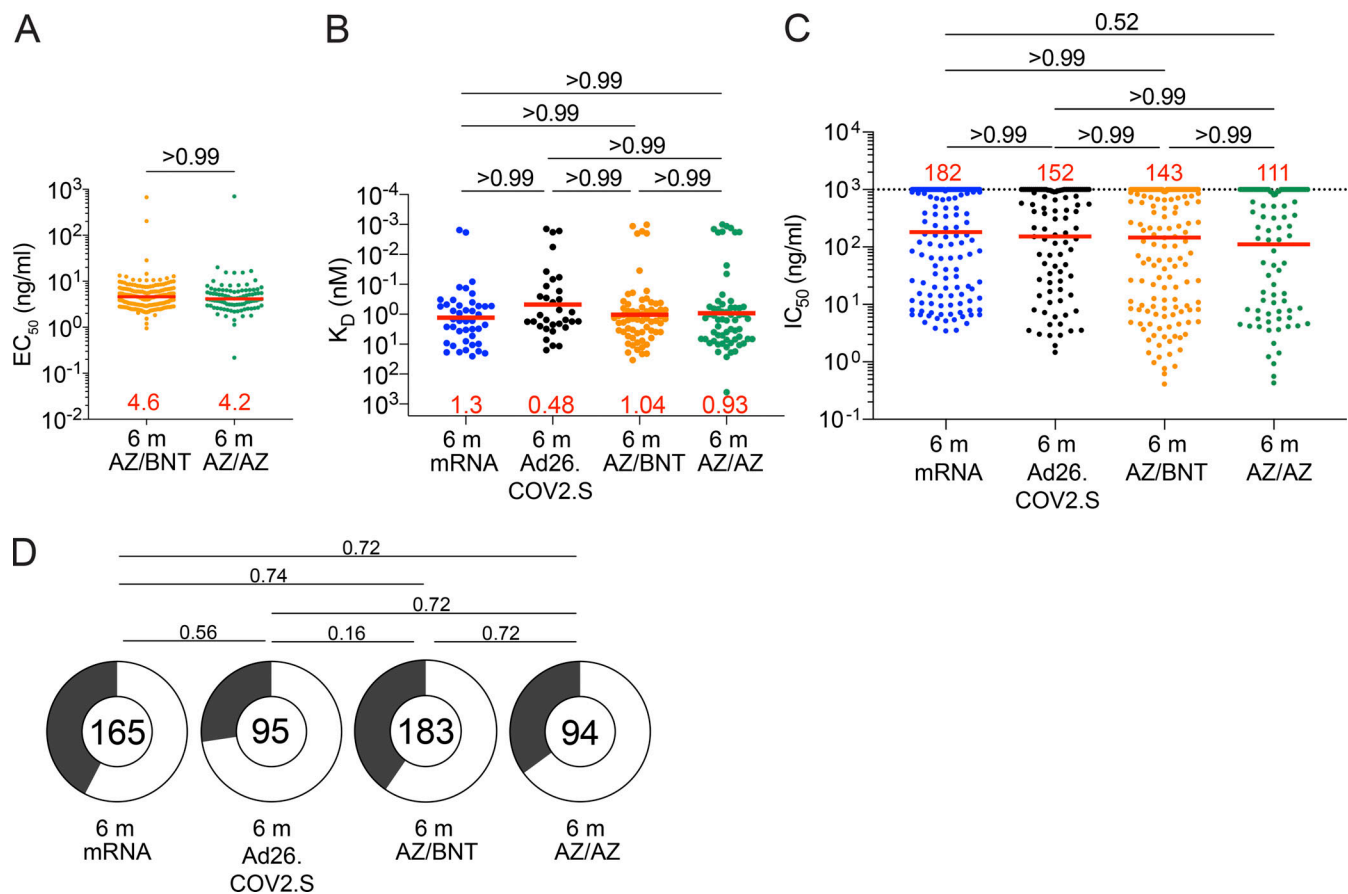
Wang et al.
In-depth immunological COVID-19 vaccine comparison

Journal of Experimental Medicine 5 of 15
https://doi.org/10.1084/jem.20220826

Figure 3. **Anti–SARS-CoV-2 mAbs. (A)** Graph shows EC_{50} of $n = 277$ Wuhan-Hu-1 RBD-binding mAbs measured by ELISA against Wuhan-Hu-1 RBD from AZ/BNT ($n = 183$) and AZ/AZ ($n = 94$) vaccinees. **(B)** Graph showing affinity measurements ($K_{D}s$) for Wuhan-Hu-1 RBD measured by BLI for antibodies cloned from mRNA vaccinees 6 mo (m) after initial dose ($n = 43$; Cho et al., 2021) and from Ad26.COV2.S vaccinees 6 mo ($n = 33$) after prime (Cho et al., 2022) compared to antibodies cloned from AZ/BNT ($n = 189$) and AZ/AZ ($n = 94$) vaccinees 6 mo after initial dose. **(C)** Graphs show anti–SARS-CoV-2 neutralizing activity of mAbs measured by a SARS-CoV-2 pseudotype virus neutralization assay using WT (Wuhan-Hu-1[Wu et al., 2020]; SARS-CoV-2 pseudovirus [Robbiani et al., 2020; Schmidt et al., 2020]) for antibodies cloned from mRNA vaccinees and 6 mo after initial dose ($n = 262$; Cho et al., 2021) or from Ad26.COV2.S vaccinees ($n = 95$) 6 mo after prime (Cho et al., 2022) compared to antibodies cloned from AZ/BNT ($n = 189$) and AZ/AZ ($n = 94$) vaccinees 6 mo after initial dose. **(D)** Pie charts indicated the frequency of neutralizing ($IC_{50} < 1,000$ ng/ml, white) vs. non-neutralizing ($IC_{50} > 1,000$ ng/ml, black) antibodies cloned from mRNA vaccinees (Cho et al., 2021), Ad26.COV2.S vaccinees (Cho et al., 2022), AZ/AZ vaccinees, and AZ/BNT vaccinees. All experiments were performed at least in duplicate. Red bars and lines indicate geometric mean values. Statistical significance in A–C was determined by two-tailed Kruskal–Wallis test with subsequent Dunn's multiple comparisons. Pie charts were compared using a two-tailed Fisher's exact test.

neutralizing to non-neutralizing antibodies for all four regimens was not significantly different (Fig. 3 D). We conclude that memory B cells present in circulation 6 mo after initial mRNA, Ad26.COV2.S, AZ/AZ, and AZ/BNT vaccine doses express antibodies with similar binding affinities and have a neutralizing potency against Wuhan-Hu-1 SARS-CoV-2.

Epitopes and neutralizing breadth
SARS-CoV-2 infection and vaccination elicit anti-RBD antibodies that target four structurally defined classes of epitopes on the RBD (Barnes et al., 2020; Muecksch et al., 2022; Muecksch et al., 2021; Wang et al., 2021c; Yuan et al., 2020). Class 1 and 2 antibodies block ACE2 binding directly, and Class 3 and 4 antibodies target more conserved regions on the RBD (Gaebler et al., 2021; Muecksch et al., 2022; Muecksch et al., 2021; Wang et al., 2021c). Class 1 and 2 antibodies develop early after infection or mRNA-immunization (Muecksch et al., 2022), while Ad26.COV2.S

vaccination leads to a more diverse, early memory B cell response that is dominated by Class 3 and 4 antibodies (Cho et al., 2022). Nevertheless, continued memory B cell evolution results in comparable epitope specificities 5–6 mo after the initial mRNA or Ad26.COV.2S immunization (Cho et al., 2022).

To define the epitopes recognized by anti-RBD memory antibodies elicited by AZ/BNT or AZ/AZ vaccination, we performed BLI competition experiments. A preformed antibody-RBD-complex was exposed to a second antibody targeting one of the four classes of structurally defined epitopes (Barnes et al., 2020; Robbiani et al., 2020; C105 as Class 1; C144 as Class 2; C135 as Class 3; and CR3022 as Class 4). We examined 128 RBD-binding antibodies randomly obtained from the AZ/BNT ($n = 66$) and AZ/AZ ($n = 62$) vaccinees. This included AZ/BNT ($n = 44$) and AZ/AZ ($n = 39$) antibodies with $IC_{50}s$ <1,000 ng/ml.

The epitope distribution of the memory antibody repertoires was significantly different between all four vaccine regimens

(Fig. S4 B). Moreover, the overall epitope specificities of the antibody repertoires were significantly different between mRNA vaccinees and AZ/BNT or AZ/AZ vaccinees (Fig. 4 A). This was particularly evident among neutralizing (IC$_{50}$ < 1,000 ng/ml) antibodies for which the frequency of antibodies that target unknown epitopes (non-classified) was highly enriched in the antibody repertoire isolated from AZ/BNT or AZ/AZ vaccinees (Fig. 4 A). At the same time, there were no significant differences in epitope specificities for non-neutralizing (IC$_{50}$ > 1,000 ng/ml) antibodies.

To examine the contribution of the different antibody classes to the neutralizing potency and breadth elicited by each of the four vaccine regimens, we regrouped the antibodies as follows: (1) antibodies targeting Class 1 and/or 2 epitopes; (2) antibodies additionally or exclusively targeting Class 3 epitopes; (3) antibodies additionally or exclusively targeting Class 4 epitopes; or (4) non-classifiable antibodies. While the neutralizing potency of the first 3 groups was comparable among all four vaccine regimens, AZ/BNT and AZ/AZ vaccination elicited non-classifiable antibodies that were significantly more potent than their mRNA or Ad26.COV.2S counterparts (Fig. 4 B).

To determine the neutralizing breadth of the memory antibodies that developed after AZ/BNT or AZ/AZ vaccination, we analyzed a panel of randomly selected Wuhan-Hu-1 (WT)–neutralizing antibodies from AZ/BNT and AZ/AZ vaccinees (AZ/BNT: n = 32, and AZ/AZ: n = 34) for the neutralizing activity against SARS-CoV-2 pseudoviruses carrying amino acid substitutions specific to the Delta and Omicron BA.1-RBD.

78% of the AZ/BNT- and 82% of the AZ/AZ-elicited antibodies neutralized SARS-CoV-2 pseudoviruses carrying the Delta RBD-amino acid substitutions, some with IC$_{50}$ values of <10 ng/ml (Fig. 4 C and Table S4). Omicron BA.1 showed the highest degree of neutralization resistance; nevertheless 8 out of 32 antibodies isolated from AZ/BNT and 14 out of 34 antibodies isolated from AZ/AZ vaccinees neutralized this variant. Some of the most potent Omicron-neutralizing antibodies targeted epitopes that could not be classified in our BLI experiments (non-classified) with IC$_{50}$s below 10 ng/ml (Fig. 4, C and D; and Table S4). 5 out of 32 AZ/BNT- and 10 out of 34 AZ/AZ- antibodies neutralized both Delta and Omicron, a proportion that was not significantly different compared to antibodies elicited by other vaccine regimens (Fig. 4, C and E).

We conclude that the relative distribution of RBD epitopes targeted by neutralizing antibodies expressed by memory B cells that develop after mRNA, Ad26.COV.2S, or ChAdOx1 vaccination regimens differ significantly.

Structural analysis of antibody–RBD interaction

To understand the interaction between these non-classified antibodies and RBD, we imaged WT Wuhan-Hu-1 SARS-CoV-2 S 6P bound to Fab fragments of a potent and broad AZ/AZ antibody (AZ090) by single-particle cryo-electron microscopy (cryo-EM; Fig. 5 A and Fig. S5, A–F). The resolution of the reconstituted cryo-EM electron density map was 3.02 Å for the whole complex and 3.85 Å for the RBD-AZ090. Structural analyses of the density maps showed that the binding orientation of AZ090 is similar to previously described potent antibodies

that were isolated following natural infection (Dejnirattisai et al., 2021; Reincke et al., 2022; Tortorici et al., 2020; Wang et al., 2021a; Fig. S5 G). AZ090 and this type of antibodies share the same immunoglobulin heavy and light chain genes (IGHV1-58 and IGKV3-20/IGKJ; Fig. S5, H and I). Unlike Class 1 antibodies, the footprint of AZ90 is located in the ridge region of RBD with more limited overlap with Omicron (BA.1) amino acid substitutions than typical class 1 (C105) and class 2 (C144) antibodies (Fig. 5 B). The distinctive binding pattern of AZ090 may also explain the lack of competition in BLI experiments and the neutralizing breadth across different SARS-CoV-2 variants.

Discussion

Neutralizing antibodies are correlates of vaccine efficacy in protection against SARS-CoV-2 infection and severe COVID-19 (Bergwerk et al., 2021; Feng et al., 2021; Khoury et al., 2021; Li et al., 2022). All three US-authorized vaccines have shown substantial protection against SARS-CoV-2 infection, hospitalization, and death (Botton et al., 2022; Self et al., 2021). However, vaccine efficacy wanes over time with a prominent loss of protection against infection after the Ad26.COV.2S vaccine compared to mRNA (Lin et al., 2022). Similarly, vaccination regimens with the globally predominant ChAdOx1 vaccine have been less effective in the protection against infection and symptomatic COVID-19 compared to mRNA vaccination (Andrews et al., 2022; Braeye et al., 2022). However, the combination of a ChAdOx1 prime and a second mRNA dose shows similar levels of protection as two-dose mRNA vaccination (Nordstrom et al., 2021).

Our comparative analysis of plasma and memory B cell antibodies provides a mechanistic explanation for the observed real-world protective efficacy of several different vaccine regimens. Binding and neutralizing antibody levels elicited by two-dose mRNA or AZ/BNT vaccination exceed those elicited by AZ/AZ or single-dose Ad26.COV.2S vaccination. Of note, our finding that age- and RBD-binding antibodies inversely correlated in the AZ/AZ cohort suggests that even minor age differences between study cohorts could potentially contribute to observed differences in plasma and memory B cell antibody responses.

Omicron BA.1 neutralization was highest after AZ/BNT vaccination, suggesting that combination vaccine protocols with extended dosing intervals may induce improved plasma-neutralizing responses. In line with our observation, vaccine efficacy has been shown to increase with the interval between the first and second vaccine doses (Voysey et al., 2021). Prolonged affinity maturation yielding higher affinity B cells for plasma cell maturation upon the administration of the second vaccine dose may be of importance in this process (Hall et al., 2022). However, improved plasma-neutralizing responses in AZ/BNT vaccinees appeared relatively short-lived as Omicron BA.1–neutralizing titers were not statistically different from mRNA or AZ/AZ vaccinees at 6 mo after the prime.

The relative potency and breadth, i.e., neutralizing activity against Delta and Omicron, of memory B cell antibodies produced by the four different vaccine regimens were overall
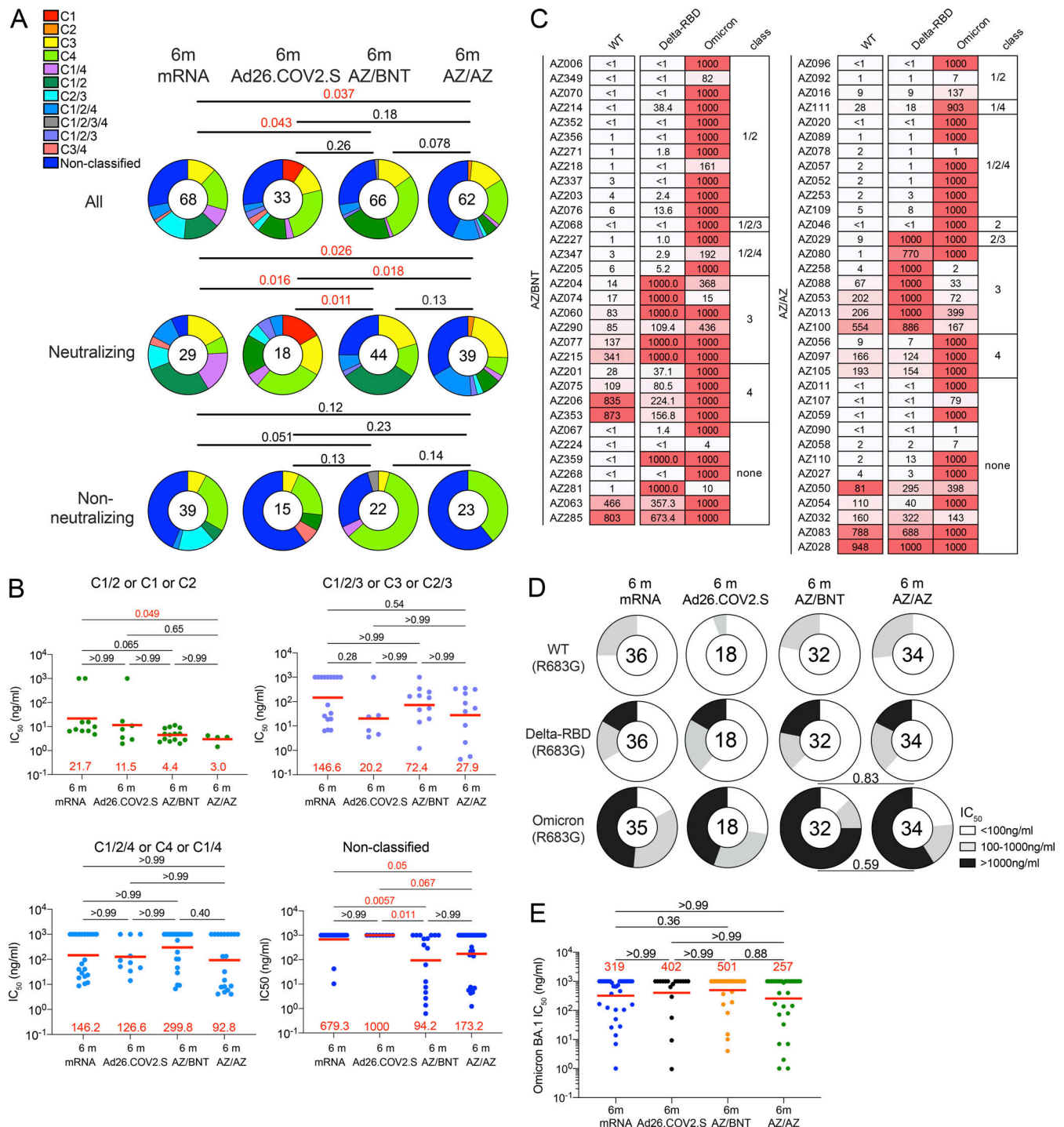
Wang et al.
In-depth immunological COVID-19 vaccine comparison

Journal of Experimental Medicine   7 of 15
https://doi.org/10.1084/jem.20220826

Figure 4. **Epitopes and neutralizing breadth.** Results of epitope mapping performed by competition BLI, comparing mAbs cloned from Ad26.COV.2S vaccinees 6 mo (m; $n = 33$) after prime (Cho et al., 2022) and mAbs cloned from mRNA vaccinees 6 mo after initial dose ($n = 68$; Cho et al., 2021), to mAbs cloned from AZ/AZ ($n = 62$) or AZ/BNT($n = 66$) vaccinees 6 mo after initial dose. **(A)** Pie charts show the distribution of the antibody classes among all RBD-binding antibodies, Wuhan-Hu-1–neutralizing antibodies only, or non-neutralizing antibodies only. Statistical significance was determined by using a two-tailed Chi-square test. **(B)** Graphs showing IC_{50} neutralization activity of antibodies indicated in A and Fig. S5 A, with four categories by combining (1) C1/2 or C1 or C2 as C1/2; (2) C1/2/3 or C3 or C2/3 as C1/2/3; (3) C1/2/4 or C4 or C1/4 as C1/2/4; (4) non-classified and C1/2/3/4 as non-classified. **(C)** Heatmaps show IC_{50}s of antibodies obtained from AZ/BNT vaccinees ($n = 32$), and AZ/BNT vaccinees ($n = 34$), against indicated mutant and variant SARS-CoV-2 pseudoviruses listed across the top. Delta-RBD indicate the L452R/T478K and Omicron BA.1. The deletions/substitutions corresponding to viral variants were incorporated into a spike protein that also includes the R683G substitution, which disrupts the furin cleavage site and increases particle infectivity. **(D)** Pie charts show fraction of potent neutralizing ($IC_{50} < 100$ ng/ml), less potent neutralizing (100 ng/ml < $IC_{50} < 1,000$ ng/ml), and non-neutralizing ($IC_{50} > 1,000$ ng/ml) antibodies in white, light, and dark gray, respectively, for indicated SARS-CoV-2 pseudoviruses. Number in inner circles indicates the number of antibodies tested. **(E)** Graphs showing IC_{50} neutralization activity of antibodies mAbs cloned from Ad26.COV.2S vaccinees at 6 mo ($n = 18$) after prime (Cho et al., 2022) and mAbs cloned

Wang et al.
In-depth immunological COVID-19 vaccine comparison

Journal of Experimental Medicine   8 of 15
https://doi.org/10.1084/jem.20220826

from mRNA vaccinees at 6 mo after initial dose (n = 35; Cho et al., 2021), to mAbs cloned from AZ/AZ (n = 34) or AZ/BNT(n = 32) vaccinees 6 mo after initial dose, against Omicron BA.1. Red bars and lines indicated geometric mean values. All experiments were performed at least in duplicate. Statistical significance in A was determined by two-tailed Kruskal–Wallis test with subsequent Dunn's multiple comparisons in B and E. Statistical significance was determined using a two-tailed Chi-square test.

similar. However, they differed in the frequency of memory cells and the distribution of the RBD epitopes targeted by mRNA, Ad26.COV.2S, and ChAdOx1 vaccination regimens. Differences in dosing intervals between prime and boost immunization, distinct antigenic features of the full-length WT SARS-CoV-2 spike protein lacking prefusion-stabilizing mutations in the ChAdOx1 vaccine (Tortorici and Veesler, 2019), and the precise biochemistry of the antigen and its presentation may all contribute to these observations.

Notably and in line with previous reports (Kaku et al., 2022; Zhang et al., 2022), the frequency of RBD-binding memory cells that develop after two-dose mRNA vaccination was greater than vaccination regimens that are based on adenoviral vectors at 6 mo after vaccination. The latter is likely to be particularly important for recall responses and protection from severe diseases upon repeated viral challenges (Amanna et al., 2007; Mesin et al., 2020).

Materials and methods
Study participants
Healthcare workers receiving routine COVID-19 vaccination were enrolled in the EICOV and COVIM prospective observational cohort studies conducted at Charité–Universitätsmedizin Berlin (Berlin, Germany) after written informed consent was obtained. EICOV was approved by the ethics committee of Charité–Universitätsmedizin Berlin (EA4/245/20), and COVIM was approved by the Federal Institute for Vaccines and Biomedicines (Paul Ehrlich Institute) and by the ethics committee of the state of Berlin (EudraCT-2021–001512–28). Both studies were conducted in accordance with the guidelines of Good Clinical Practice (ICH 1996) and the Declaration of Helsinki.

Healthcare workers at Charité–Universitätsmedizin Berlin were offered either two doses of BNT162b2 3 wk apart or an initial dose of ChAdOx1 nCov-19 followed by a heterologous boost with BNT162b2 10–12 wk later. The vaccine regimen depended on availability and current official recommendations. Healthcare workers who received an initial dose of ChAdOx1 nCov-19 were also free to choose a homologous booster with ChAdOx1 nCov-19 10–12 wk later (Hillus et al., 2021). Plasma samples were tested for binding activity toward the nucleocapsid protein (N; 40588-V08B; Sino Biological) of SARS-CoV-2. The absence of seroconversion toward N during the study interval was used to exclude SARS-CoV-2 infection, in addition to participants' reported history. For detailed participant characteristics, see Table S1 and previous publications (Cho et al., 2021; Cho et al., 2022; Muecksch et al., 2022). Cohort sample analyses were performed under an existing Rockefeller University IRB-approved protocol (DRO-1006).

Blood samples processing and storage
Blood samples were collected in Heparin and serum-gel monovette tubes (Greiner Bio-One). Peripheral blood mononuclear cells were isolated by gradient centrifugation and stored in liquid nitrogen in the presence of FCS and DMSO. Heparinized plasma and serum samples were fractioned by centrifugation, aliquoted, and stored at –80°C until analysis. Prior to experiments, aliquots of plasma samples were heat-inactivated (56°C for 30 min) and then stored at 4°C.

ELISAs
ELISAs (Amanat et al., 2020; Grifoni et al., 2020) to evaluate antibodies binding to SARS-CoV-2 RBD were performed by coating high-binding 96-half-well plates (3690; Corning) with
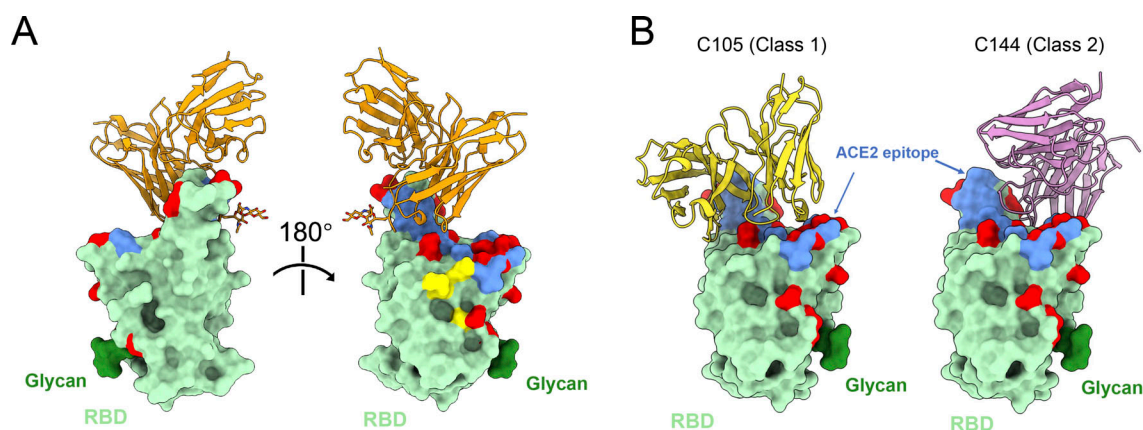

Figure 5.   **Structural analysis of AZ090 antibody. (A)** RBD of SARS-CoV-2 is shown as surface and colored green. Fab of AZ090 fab is colored orange, ACE2 epitope is colored blue, and N343 glycan is colored dark green. Omicron (BA.1) mutations are colored red. **(B)** As in A. C105 (Class 1 antibody, PDB: 6XCM) is colored yellow, and C144 (Class 2 antibody, PDB: 7K90) is colored pink.

50 µl per well of a 1 µg/ml protein solution in PBS overnight at 4°C. Plates were washed six times with washing buffer (1× PBS with 0.05% Tween-20; Sigma-Aldrich) and incubated with 170 µl per well-blocking buffer (1× PBS with 2% BSA and 0.05% Tween-20; Sigma-Aldrich) for 1 h at room temperature. Immediately after blocking, mAbs or plasma samples were added to PBS and incubated for 1 h at room temperature. Plasma samples were assayed at a 1:66 starting dilution and 10 additional threefold serial dilutions. mAbs were tested at 10 µg/ml starting concentration and 10 additional fourfold serial dilutions. Plates were washed six times with washing buffer and then incubated with anti-human IgG, IgM, or IgA secondary antibody conjugated to horseradish peroxidase (HRP; 109-036-088, 109-035-129; Jackson ImmunoResearch, and A0295; Sigma-Aldrich) in blocking buffer at a 1:5,000 dilution (IgM and IgG) or 1:3,000 dilution (IgA). Plates were developed by the addition of the HRP substrate, 3,3′,5,5′-tetramethylbenzidine (TMB; Thermo Fisher Scientific) for 10 min (plasma samples) or 4 min (mAbs). The developing reaction was stopped by adding 50 µl of 1 M H_2SO_4, and absorbance was measured at 450 nm with an ELISA microplate reader (FluoStar Omega; BMG Labtech) with Omega and Omega MARS software for analysis. For plasma samples, a positive control (plasma from participant COV72, diluted 66.6-fold and ten additional threefold serial dilutions in PBS) was added to every assay plate for normalization. The average of its signal was used for normalization of all the other values on the same plate with Excel software before calculating the area under the curve (AUC) using Prism V9.1 (GraphPad). Negative controls of pre-pandemic plasma samples from healthy donors were used for validation (for more details, please see Robbiani et al. [2020]). For mAbs, the EC_{50} was determined using a four-parameter nonlinear regression (GraphPad Prism V9.1). EC_{50}s above 1,000 ng/ml were considered non-binders.

Proteins
The mammalian expression vector encoding the RBD of SARS-CoV-2 (GenBank MN985325.1; Spike (S) protein residues 319–539) was previously described (Barnes et al., 2020). A mammalian expression vector encoding the SARS-CoV-2 Wuhan-Hu-1 NTD (GenBank MN985325.1; S protein residues 14–307) was previously described (Wang et al., 2022a Preprint).

SARS-CoV-2 pseudotyped reporter virus
A panel of plasmids expressing RBD-mutant SARS-CoV-2 spike proteins in the context of pSARS-CoV-2-S $_{\Delta 19}$ has been described (Cho et al., 2021; Muecksch et al., 2021; Wang et al., 2021d; Weisblum et al., 2020). Variant pseudoviruses resembling SARS-CoV-2 variants Delta (B.1.617.2) and Omicron BA.1 (B.1.1.529) have been described before (Cho et al., 2021; Schmidt et al., 2022; Wang et al., 2021c) and were generated by the introduction of substitutions using synthetic gene fragments (IDT) or overlap extension PCR-mediated mutagenesis and Gibson assembly. Specifically, the variant-specific deletions and substitutions introduced were as follows: Delta: T19R, Δ156-158, L452R, T478K, D614G, P681R, D950N; Delta-RBD: L452R, T478K; Omicron BA.1: A67V, Δ69-70, T95I, G142D, Δ143-145, Δ211, L212I, ins214EPE, G339D, S371L, S373P, S375F, K417N, N440K, G446S,

S477N, T478K, E484A, Q493K, G496S, Q498R, N501Y, Y505H, T547K, D614G, H655Y, H679K, P681H, N764K, D796Y, N856K, Q954H, N969H, N969K, and L981F.

Deletions/substitutions corresponding to variants of concern listed above were incorporated into a spike protein that also includes the R683G substitution, which disrupts the furin cleavage site and increases particle infectivity. Neutralizing activity against mutant pseudoviruses was compared to a WT SARS-CoV-2 spike sequence (NC_045512), carrying R683G where appropriate.

SARS-CoV-2 pseudotyped particles were generated as previously described (Robbiani et al., 2020; Schmidt et al., 2020). Briefly, 293T (11268; CRL) cells were obtained from ATCC and the cells were transfected with pNL4-3 ΔEnv-nanoluc and pSARS-CoV-2-S$_{\Delta 19}$. Particles were harvested 48 h after transfection, filtered, and stored at –80°C.

Pseudotyped virus neutralization assay
Four- to fivefold serially diluted pre-pandemic negative control plasma from healthy donors and plasma from study participants were incubated with SARS-CoV-2 pseudotyped virus for 1 h at 37°C. The mixture was subsequently incubated with 293T$_{Ace2}$ cells (Robbiani et al., 2020; for all WT neutralization assays) or HT1080Ace2 cl14 (for all mutant panels and variant neutralization assays) cells (Wang et al., 2021d) for 48 h after which cells were washed with PBS and lysed with Luciferase Cell Culture Lysis 5× reagent (Promega). Nanoluc Luciferase activity in lysates was measured using the Nano-Glo Luciferase Assay System (Promega) with the Glomax Navigator (Promega) or ClarioStar Microplate Multimode Reader (BMG). The relative luminescence units were normalized to those derived from cells infected with SARS-CoV-2 pseudotyped virus in the absence of plasma or mAbs. The half-maximal neutralization titers for plasma (NT$_{50}$) or half-maximal and 90% inhibitory concentrations for mAbs (IC$_{50}$ and IC$_{90}$) were determined using four-parameter nonlinear regression (least squares regression method without weighting; constraints: top = 1, bottom = 0; GraphPad Prism).

Biotinylation of viral protein for use in flow cytometry
Purified and Avi-tagged SARS-CoV-2 Wuhan-Hu-1 RBD and NTD were biotinylated using the Biotin-Protein Ligase-BIRA kit according to the manufacturer's instructions (Avidity) as described before (Robbiani et al., 2020). Ovalbumin (A5503-1G; Sigma-Aldrich) was biotinylated using the EZ-Link Sulfo-NHS-LC-Biotinylation kit according to the manufacturer's instructions (Thermo Fisher Scientific). Biotinylated ovalbumin was conjugated to streptavidin-BB515 (564453; BD). RBD was conjugated to streptavidin-PE (554061; BD Biosciences) and streptavidin-AF647 (405237; Biolegend; Robbiani et al., 2020). NTD was conjugated to streptavidin-BV421 (405225; Biolegend) and streptavidin-BV711 (563262; BD Biosciences).

Flow cytometry and single-cell sorting
Single-cell sorting by flow cytometry was described previously (Robbiani et al., 2020). Briefly, peripheral blood mononuclear cells were enriched for B cells by negative selection using a pan–B-cell isolation kit according to the manufacturer's

instructions (130-101-638; Miltenyi Biotec). The enriched B cells were incubated in FACS buffer (1× PBS, 2% FCS, 1 mM EDTA) with the following anti-human antibodies (all at 1:200 dilution): anti-CD20-PECy7 (335793; BD Biosciences), anti-CD3-APC-eFluro780 (47-0037-41; Invitrogen), anti-CD8-APC-eFluor780 (47-0086-42; Invitrogen), anti-CD16-APC-eFluor780 (47-0168-41; Invitrogen), anti-CD14-APC-eFluor780 (47-0149-42; Invitrogen), as well as Zombie NIR (423105; BioLegend) and fluorophore-labeled Wuhan-Hu-1 RBD, NTD, and ovalbumin (Ova) for 30 min on ice. AccuCheck Counting Beads (PCB100; Life Technologies) were added to each sample according to the manufacturer's instructions. Single $CD3^-CD8^-CD14^-CD16^-CD20^+Ova^-$ B cells that were $RBD^-PE^+RBD^-AF647^+$ were sorted into individual wells of 96-well plates containing 4 µl of lysis buffer (0.5× PBS, 10 mM dithiothreitol, 3,000 units/ml RNasin ribonuclease inhibitors [N2615; Promega]) per well using a FACS Aria III and FACSDiva software (Becton Dickinson) for acquisition and FlowJo for analysis. The sorted cells were frozen on dry ice and then stored at –80°C or immediately used for subsequent RNA reverse transcription.

Antibody sequencing, cloning, and expression
Antibodies were identified and sequenced as described previously (Robbiani et al., 2020; Wang et al., 2021b). In brief, RNA from single cells was reverse-transcribed (SuperScript III Reverse Transcriptase, 18080-044; Invitrogen) and the cDNA was stored at –20°C or used for subsequent amplification of the variable IGH, IGL, and IGK genes by nested PCR and Sanger sequencing. Sequence analysis was performed using MacVector. Amplicons from the first PCR reaction were used as templates for sequence- and ligation-independent cloning into antibody expression vectors. Recombinant mAbs were produced and purified as previously described (Robbiani et al., 2020).

BLI
BLI assays were performed as previously described (Robbiani et al., 2020). Briefly, we used the Octet Red instrument (ForteBio) at 30°C with shaking at 1,000 r.p.m. Epitope binding assays were performed with protein A biosensor (18-5010; ForteBio) following the manufacturer's protocol "classical sandwich assay" as follows: (1) sensor check: sensors immersed 30 s in buffer alone (buffer 18-1105; ForteBio); (2) capture first Ab: sensors immersed 10 min with Ab1 at 10 µg/ml; (3) baseline: sensors immersed 30 s in buffer alone; (4) blocking: sensors immersed 5 min with IgG isotype control at 10 µg/ml; (5) baseline: sensors immersed 30 s in buffer alone; (6) antigen association: sensors immersed 5 min with RBD at 10 µg/ml; (7) baseline: sensors immersed 30 s in buffer alone; and (8) association Ab2: sensors immersed 5 min with Ab2 at 10 µg/ml. Affinity measurements of anti–SARS-CoV-2 IgGs binding were corrected by subtracting the signal obtained from traces performed with IgGs in the absence of RBD. The kinetic analysis using protein A biosensor (18-5010; ForteBio) was performed as follows: (1) baseline: 60 s immersion in buffer; (2) loading: 200 s immersion in a solution with IgGs 10 µg/ml; (3) baseline: 200 s immersion in buffer; (4) association: 300 s immersion in solution with RBD at 20, 10, or 5 µg/ml; and (5) dissociation: 600 s

immersion in buffer. Curve fitting was performed using a fast 1:1 binding model and the data analysis software (ForteBio). Mean K_D values were determined by averaging all binding curves that matched the theoretical fit with an R^2 value ≥0.8. Curve fitting was performed using the Fortebio Octet Data analysis software (ForteBio).

Recombinant protein expression
Stabilized SARS-CoV-2 6P ectodomain and Fabs were expressed and purified as previously described (Wang et al., 2022b). Briefly, constructs encoding the stabilized spike of SARS-CoV-2 ectodomain (Hsieh et al., 2020) were used to transiently transfect Expi293F cells (Gibco). Supernatants were harvested after 4 d, and S 6P proteins were purified by nickel affinity following size-exclusion chromatography. Peak fractions from size-exclusion chromatography were identified by native gel analysis for spike trimer fractions.

Cryo-EM sample preparation
Purified Fabs were mixed with S 6P protein at a 1.1:1 M ratio of Fab-to-protomer for 30 min at room temperature. Fab-S complexes were deposited on a freshly glow-discharged 400 mesh, 1.2/1.3 Quantifoil grid (Electron Microscopy Sciences). Immediately before the deposition of 3 ml of the complex onto the grid, fluorinated octyl-maltoside (Anatrace) was added to the sample to a final concentration of 0.02% w/v. Samples were vitrified in 100% liquid ethane using a Mark IV Vitrobot (Thermo Fisher Scientific) after blotting at 22°C and 100% humidity for 3 s with filter paper.

Cryo-EM data collection and processing
Single-particle cryo-EM data were collected on a Titan Krios transmission electron microscope (Thermo Fisher Scientific) equipped with a Gatan K3 direct detector, operating at 300 kV and controlled using SerialEM automated data collection software (Mastronarde, 2005). A total dose of 56.56 e/$Å^2$ was accumulated on each movie with a pixel size of 0.515 and a defocus range of –0.8 and –2.0 µm. Movie frame alignment, contrast transfer function estimation, particle picking, and extraction were carried out using cryoSPARC v3.3.1 (Punjani et al., 2017). Reference-free particle picking and extraction were performed on dose-weighted micrographs. A subset of 4×-downsampled particles was used to conduct several rounds of reference-free 2D classification, then the selected Fab-S particles were extracted and 2×-downsampled, yielding a pixel size of 1.03 Å. The particles were used to generate ab initio models, which were then used for heterogeneous refinement of the entire dataset in cryoSPARC. Particles belonging to classes that resembled Fab-S structures were homogeneously refined following non-uniform refinement until imported into Relion 3.1.3 for contrast transfer function refinement. The particles were then imported into cryoSPARC for heterogeneous refinement. Particles belonging to classes with better Fab density were selected and subjected to another round of homogeneous refinement following with non-uniform refinement. To improve the density of the RBD/AZ090 interface, several rounds of local refinement were then performed using different soft masks. Reported resolutions are based on the gold-standard Fourier shell correlation of 0.143 criteria (Bell et al., 2016).

Cryo-EM structure modeling and analysis

UCSF Chimera (Pettersen et al., 2004) and Coot (Emsley et al., 2010) were used to fit atomic models into the locally refined cryoEM map. Models were refined and validated by Phenix (Liebschner et al., 2019). Figures were generated using UCSF ChimeraX (Goddard et al., 2018).

Computational analyses of antibody sequences

Antibody sequences were trimmed based on quality and annotated using Igblastn v.1.14. with IMGT domain delineation system. Annotation was performed systematically using Change-O toolkit v.0.4.540 (Gupta et al., 2015). Clonality of heavy and light chains was determined using DefineClones.py implemented by Change-O v0.4.5 (Gupta et al., 2015). The script calculates the Hamming distance between each sequence in the data set and its nearest neighbor. Distances are subsequently normalized and account for differences in junction sequence length, and clonality is determined based on a cut-off threshold of 0.15. Heavy and light chains derived from the same cell were subsequently paired, and clonotypes were assigned based on their V and J genes using in-house R and Perl scripts. All scripts and the data used to process antibody sequences are publicly available on GitHub (https://github.com/stratust/igpipeline/tree/igpipeline2_timepoint_v2).

The frequency distributions of human V genes in anti–SARS-CoV-2 antibodies from this study were compared to 131,284,220 IgH and IgL sequences generated by Soto et al. (2019) and downloaded from cAb-Rep (Guo et al., 2019), a database of human-shared BCR clonotypes available at https://cab-rep.c2b2.columbia.edu/. Based on the 150 distinct V genes that make up the 1,099 analyzed sequences from the Ig repertoire of the six participants present in this study, we selected the IgH and IgL sequences from the database that are partially coded by the same V genes and counted them according to the constant region. The frequencies shown in Fig. S4 are relative to the source and isotype analyzed. We used the two-sided binomial test to check whether the number of sequences belonging to a specific IGHV or IGLV gene in the repertoire is different according to the frequency of the same IgV gene in the database. Adjusted P values were calculated using the false discovery rate (FDR) correction. Significant differences are denoted with stars.

Nucleotide somatic hypermutation and the length of the complementarity-determining region 3 (CDR3) were determined using in-house R and Perl scripts. For somatic hypermutations, IGHV and IGLV nucleotide sequences were aligned against their closest germlines using Igblastn, and the number of differences was considered nucleotide mutations. The average number of mutations for V genes was calculated by dividing the sum of all nucleotide mutations across all participants by the number of sequences used for the analysis.

Data presentation

Figures were arranged in Adobe Illustrator 2022.

Online supplemental material

Fig. S1 shows patients' demographics and correlations between plasma activity after vaccination and clinical parameters. Fig. S2 shows a flow cytometry gating strategy to phenotype or sort RBD- and NTD-binding memory B cells after vaccination. Fig. S3 shows the frequency of V gene usage of RBD-binding memory B cells after vaccination. Fig. S4 shows additional information on antibodies' binding epitopes. Fig. S5 shows processing data for cryo-EM. Table S1 details the individual characteristics of participants who received AZ/AZ or AZ/BNT vaccines. Table S2 details sequence information of all characterized RBD-binding memory B cells from AZ/AZ or AZ/BNT vaccinated individuals. Table S3 provides information of all recombinant mAbs cloned from RBD-binding B cells. Table S4 provides information on neutralization breadth against a panel of variants that were tested on the selected number of recombinant mAbs. Table S5 provides parameters for cryo-EM.

Data availability

Data are provided in Tables S1, S2, S3, S4, and S5. The raw sequencing data and computer scripts associated with Fig. 2 have been deposited at Github (https://github.com/stratust/igpipeline/tree/igpipeline2_timepoint_v2). This study also uses data from DeWitt et al. (2016), cAb-Rep (https://cab-rep.c2b2.columbia.edu/; Guo et al., 2019), Sequence Read Archive (accession SRP010970), and from Soto et al. (2019). The structural model and density map have been deposited in the Protein Data Bank and Electron Microscopy Data Bank under entry 8DAD and EMD-27270. Computer code to process the antibody sequences is available on GitHub (https://github.com/stratust/igpipeline/tree/igpipeline2_timepoint_v2).

References

Amanat, F., D. Stadlbauer, S. Strohmeier, T.H.O. Nguyen, V. Chromikova, M. McMahon, K. Jiang, G.A. Arunkumar, D. Jurczyszak, J. Polanco, et al. 2020. A serological assay to detect SARS-CoV-2 seroconversion in humans. Nat. Med. 26:1033–1036. https://doi.org/10.1038/s41591-020-0913-5

Amanna, I.J., N.E. Carlson, and M.K. Slifka. 2007. Duration of humoral immunity to common viral and vaccine antigens. N. Engl. J. Med. 357: 1903–1915. https://doi.org/10.1056/NEJMoa066092

Andrews, N., E. Tessier, J. Stowe, C. Gower, F. Kirsebom, R. Simmons, E. Gallagher, S. Thelwall, N. Groves, G. Dabrera, et al. 2022. Duration of protection against mild and severe disease by covid-19 vaccines. N. Engl. J. Med. 386:340–350. https://doi.org/10.1056/NEJMoa2115481

Barnes, C.O., C.A. Jette, M.E. Abernathy, K.A. Dam, S.R. Esswein, H.B. Gristick, A.G. Malyutin, N.G. Sharaf, K.E. Huey-Tubman, Y.E. Lee, et al. 2020. SARS-CoV-2 neutralizing antibody structures inform therapeutic strategies. Nature. 588:682–687. https://doi.org/10.1038/s41586-020-2852-1

Barros-Martins, J., S.I. Hammerschmidt, A. Cossmann, I. Odak, M.V. Stankov, G. Morillas Ramos, A. Dopfer-Jablonka, A. Heidemann, C. Ritter, M. Friedrichsen, et al. 2021. Immune responses against SARS-CoV-2 variants after heterologous and homologous ChAdOx1 nCoV-19/BNT162b2 vaccination. Nat. Med. 27:1525–1529. https://doi.org/10.1038/s41591-021-01449-9

Bednarski, E., P.M. Del Rio Estrada, J. DaSilva, C. Boukadida, F. Zhang, Y.A. Luna-Villalobos, X. Rodríguez-Rangel, E. Pitén-Isidro, E. Luna-García, D.D. Rivera, et al. 2022. Antibody and memory B-cell immunity in a heterogeneously SARS-CoV-2 infected and vaccinated population. medRxiv. https://doi.org/10.1101/2022.02.07.22270626 (Preprint posted February 8, 2022)

Bell, J.M., M. Chen, P.R. Baldwin, and S.J. Ludtke. 2016. High resolution single particle refinement in EMAN2.1. Methods. 100:25–34. https://doi.org/10.1016/j.ymeth.2016.02.018

Bergwerk, M., T. Gonen, Y. Lustig, S. Amit, M. Lipsitch, C. Cohen, M. Mandelboim, E.G. Levin, C. Rubin, V. Indenbaum, et al. 2021. Covid-19 breakthrough infections in vaccinated health care workers. N. Engl. J. Med. 385:1474–1484. https://doi.org/10.1056/NEJMoa2109072

Botton, J., L. Semenzato, M.J. Jabagi, B. Baricault, A. Weill, R. Dray-Spira, and M. Zureik. 2022. Effectiveness of Ad26.COV2.S vaccine vs BNT162b2 vaccine for COVID-19 hospitalizations. JAMA Netw. Open. 5:e220868. https://doi.org/10.1001/jamanetworkopen.2022.0868

Braeye, T., L. Catteau, R. Brondeel, J.A.F. van Loenhout, K. Proesmans, L. Cornelissen, H. Van Oyen, V. Stouten, P. Hubin, M. Billuart, et al. 2022. Vaccine effectiveness against onward transmission of SARS-CoV2-infection by variant of concern and time since vaccination, Belgian contact tracing, 2021. Vaccine. 40:3027–3037. https://doi.org/10.1016/j.vaccine.2022.04.025

Cho, A., F. Muecksch, D. Schaefer-Babajew, Z. Wang, S. Finkin, C. Gaebler, V. Ramos, M. Cipolla, P. Mendoza, M. Agudelo, et al. 2021. Anti-SARS-CoV-2 receptor-binding domain antibody evolution after mRNA vaccination. Nature. 600:517–522. https://doi.org/10.1038/s41586-021-04060-7

Cho, A., F. Muecksch, Z. Wang, T.B. Tanfous, J. DaSilva, R. Raspe, B. Johnson, E. Bednarski, V. Ramos, D. Schaefer-Babajew, et al. 2022. Antibody evolution to SARS-CoV-2 after single-dose Ad26.COV2.S vaccine in humans. J. Exp. Med. 219:e20220732. https://doi.org/10.1084/jem.20220732

Dejnirattisai, W., D. Zhou, H.M. Ginn, H.M.E. Duyvesteyn, P. Supasa, J.B. Case, Y. Zhao, T.S. Walter, A.J. Mentzer, C. Liu, et al. 2021. The antigenic anatomy of SARS-CoV-2 receptor binding domain. Cell. 184:2183–2200.e22. https://doi.org/10.1016/j.cell.2021.02.032

DeWitt, W.S., P. Lindau, T.M. Snyder, A.M. Sherwood, M. Vignali, C.S. Carlson, P.D. Greenberg, N. Duerkopp, R.O. Emerson, and H.S. Robins. 2016. A public database of memory and naive B-cell receptor sequences. PLoS One. 11:e0160853. https://doi.org/10.1371/journal.pone.0160853

Emsley, P., B. Lohkamp, W.G. Scott, and K. Cowtan. 2010. Features and development of coot. Acta Crystallogr. D Biol. Crystallogr. 66:486–501. https://doi.org/10.1107/S0907444910007493

Feng, S., D.J. Phillips, T. White, H. Sayal, P.K. Aley, S. Bibi, C. Dold, M. Fuskova, S.C. Gilbert, I. Hirsch, et al. 2021. Correlates of protection against symptomatic and asymptomatic SARS-CoV-2 infection. Nat. Med. 27: 2032–2040. https://doi.org/10.1038/s41591-021-01540-1

Gaebler, C., Z. Wang, J.C.C. Lorenzi, F. Muecksch, S. Finkin, M. Tokuyama, A. Cho, M. Jankovic, D. Schaefer-Babajew, T.Y. Oliveira, et al. 2021. Evolution of antibody immunity to SARS-CoV-2. Nature. 591:639–644. https://doi.org/10.1038/s41586-021-03207-w

GeurtsvanKessel, C.H., D. Geers, K.S. Schmitz, A.Z. Mykytyn, M.M. Lamers, S. Bogers, S. Scherbeijn, L. Gommers, R.S.G. Sablerolles, N.N. Nieuwkoop, et al. 2022. Divergent SARS-CoV-2 Omicron-reactive T and B cell responses in COVID-19 vaccine recipients. Sci. Immunol. 7:eabo2202. https://doi.org/10.1126/sciimmunol.abo2202

Goddard, T.D., C.C. Huang, E.C. Meng, E.F. Pettersen, G.S. Couch, J.H. Morris, and T.E. Ferrin. 2018. UCSF ChimeraX: Meeting modern challenges in visualization and analysis. Protein Sci. 27:14–25. https://doi.org/10.1002/pro.3235

Grifoni, A., D. Weiskopf, S.I. Ramirez, J. Mateus, J.M. Dan, C.R. Moderbacher, S.A. Rawlings, A. Sutherland, L. Premkumar, R.S. Jadi, et al. 2020. Targets of T Cell responses to SARS-CoV-2 coronavirus in humans with COVID-19 disease and unexposed individuals. Cell. 181:1489–1501.e15. https://doi.org/10.1016/j.cell.2020.05.015

Guo, Y., K. Chen, P.D. Kwong, L. Shapiro, and Z. Sheng. 2019. cAb-rep: A database of curated antibody repertoires for exploring antibody diversity and predicting antibody prevalence. Front. Immunol. 10:2365. https://doi.org/10.3389/fimmu.2019.02365

Gupta, N.T., J.A. Vander Heiden, M. Uduman, D. Gadala-Maria, G. Yaari, and S.H. Kleinstein. 2015. Change-O: A toolkit for analyzing large-scale B cell immunoglobulin repertoire sequencing data. Bioinformatics. 31: 3356–3358. https://doi.org/10.1093/bioinformatics/btv359

Hall, V.G., V.H. Ferreira, H. Wood, M. Ierullo, B. Majchrzak-Kita, K. Manguiat, A. Robinson, V. Kulasingam, A. Humar, and D. Kumar. 2022.

Delayed-interval BNT162b2 mRNA COVID-19 vaccination enhances humoral immunity and induces robust T cell responses. *Nat. Immunol.* 23:380–385. https://doi.org/10.1038/s41590-021-01126-6

Hillus, D., T. Schwarz, P. Tober-Lau, K. Vanshylla, H. Hastor, C. Thibeault, S. Jentzsch, E.T. Helbig, L.J. Lippert, P. Tscheak, et al. 2021. Safety, reactogenicity, and immunogenicity of homologous and heterologous prime-boost immunisation with ChAdOx1 nCoV-19 and BNT162b2: A prospective cohort study. *Lancet Respir. Med.* 9:1255–1265. https://doi.org/10.1016/S2213-2600(21)00357-X

Hsieh, C.L., J.A. Goldsmith, J.M. Schaub, A.M. DiVenere, H.C. Kuo, K. Javanmardi, K.C. Le, D. Wrapp, A.G. Lee, Y. Liu, et al. 2020. Structure-based design of prefusion-stabilized SARS-CoV-2 spikes. *Science.* 369:1501–1505. https://doi.org/10.1126/science.abd0826

Kaku, C.I., E.R. Champney, J. Normark, M. Garcia, C.E. Johnson, C. Ahlm, W. Christ, M. Sakharkar, M.E. Ackerman, J. Klingstrom, et al. 2022. Broad anti-SARS-CoV-2 antibody immunity induced by heterologous ChAdOx1/mRNA-1273 vaccination. *Science.* 375:1041–1047. https://doi.org/10.1126/science.abn2688

Khoury, D.S., D. Cromer, A. Reynaldi, T.E. Schlub, A.K. Wheatley, J.A. Juno, K. Subbarao, S.J. Kent, J.A. Triccas, and M.P. Davenport. 2021. Neutralizing antibody levels are highly predictive of immune protection from symptomatic SARS-CoV-2 infection. *Nat. Med.* 27:1205–1211. https://doi.org/10.1038/s41591-021-01377-8

Klok, F.A., M. Pai, M.V. Huisman, and M. Makris. 2022. Vaccine-induced immune thrombotic thrombocytopenia. *Lancet Haematol.* 9:e73–e80. https://doi.org/10.1016/S2352-3026(21)00306-9

Li, D., G.D. Sempowski, K.O. Saunders, P. Acharya, and B.F. Haynes. 2022. SARS-CoV-2 neutralizing antibodies for COVID-19 prevention and treatment. *Annu. Rev. Med.* 73:1–16. https://doi.org/10.1146/annurev-med-042420-113838

Liebschner, D., P.V. Afonine, M.L. Baker, G. Bunkoczi, V.B. Chen, T.I. Croll, B. Hintze, L.W. Hung, S. Jain, A.J. McCoy, et al. 2019. Macromolecular structure determination using X-rays, neutrons and electrons: Recent developments in Phenix. *Acta Crystallogr. D Struct. Biol.* 75:861–877. https://doi.org/10.1107/S2059798319011471

Lin, D.Y., Y. Gu, B. Wheeler, H. Young, S. Holloway, S.K. Sunny, Z. Moore, and D. Zeng. 2022. Effectiveness of covid-19 vaccines over a 9-month period in North Carolina. *N. Engl. J. Med.* 386:933–941. https://doi.org/10.1056/NEJMoa2117128

Mallapaty, S., E. Callaway, M. Kozlov, H. Ledford, J. Pickrell, and R. Van Noorden. 2021. How COVID vaccines shaped 2021 in eight powerful charts. *Nature.* 600:580–583. https://doi.org/10.1038/d41586-021-03686-x

Mastronarde, D. 2005. Automated electron microscope tomography using robust prediction of specimen movements. *J. Struct. Biol.* 152:36–51. https://doi.org/10.1016/j.jsb.2005.07.007

Mathieu, E., H. Ritchie, E. Ortiz-Ospina, M. Roser, J. Hasell, C. Appel, C. Giattino, and L. Rodes-Guirao. 2021. A global database of COVID-19 vaccinations. *Nat. Human Behav.* 5:947–953. https://doi.org/10.1038/s41562-021-01122-8

Mesin, L., A. Schiepers, J. Ersching, A. Barbulescu, C.B. Cavazzoni, A. Angelini, T. Okada, T. Kurosaki, and G.D. Victora. 2020. Restricted clonality and limited germinal center reentry characterize memory B cell reactivation by boosting. *Cell.* 180:92–106.e11. https://doi.org/10.1016/j.cell.2019.11.032

Muecksch, F., Y. Weisblum, C.O. Barnes, F. Schmidt, D. Schaefer-Babajew, Z. Wang, J C. C Lorenzi, A.I. Flyak, A.T. DeLaitsch, K.E. Huey-Tubman, et al. 2021. Affinity maturation of SARS-CoV-2 neutralizing antibodies confers potency, breadth, and resilience to viral escape mutations. *Immunity.* 54:1853–1868.e7. https://doi.org/10.1016/j.immuni.2021.07.008

Muecksch, F., Z. Wang, A. Cho, C. Gaebler, T. Ben Tanfous, J. DaSilva, E. Bednarski, V. Ramos, S. Zong, B. Johnson, et al. 2022. Increased memory B cell potency and breadth after a SARS-CoV-2 mRNA boost. *Nature.* 607:128–134. https://doi.org/10.1038/s41586-022-04778-y

Nordstrom, P., M. Ballin, and A. Nordstrom. 2021. Effectiveness of heterologous ChAdOx1 nCoV-19 and mRNA prime-boost vaccination against symptomatic covid-19 infection in Sweden: A nationwide cohort study. *Lancet Reg. Health Eur.* 11:100249. https://doi.org/10.1016/j.lanepe.2021.100249

Normark, J., L. Vikstrom, Y.D. Gwon, I.L. Persson, A. Edin, T. Bjorsell, A. Dernstedt, W. Christ, S. Tevell, M. Evander, et al. 2021. Heterologous ChAdOx1 nCoV-19 and mRNA-1273 vaccination. *N. Engl. J. Med.* 385:1049–1051. https://doi.org/10.1056/NEJMc2110716

Voysey, M., S.A. Costa Clemens, S.A. Madhi, L.Y. Weckx, P.M. Folegatti, P.K. Aley, B. Angus, V.L. Baillie, S.L. Barnabas, Q.E. Bhorat, et al. 2021.

Single-dose administration and the influence of the timing of the booster dose on immunogenicity and efficacy of ChAdOx1 nCoV-19 (AZD1222) vaccine: A pooled analysis of four randomised trials. *Lancet.* 397:881–891. https://doi.org/10.1016/S0140-6736(21)00432-3

Pettersen, E.F., T.D. Goddard, C.C. Huang, G.S. Couch, D.M. Greenblatt, E.C. Meng, and T.E. Ferrin. 2004. UCSF Chimera: A visualization system for exploratory research and analysis. *J. Comput. Chem.* 25:1605–1612. https://doi.org/10.1002/jcc.20084

Pozzetto, B., V. Legros, S. Djebali, V. Barateau, N. Guibert, M. Villard, L. Peyrot, O. Allatif, J.B. Fassier, A. Massardier-Pilonchery, et al. 2021. Immunogenicity and efficacy of heterologous ChAdOx1-BNT162b2 vaccination. *Nature.* 600:701–706. https://doi.org/10.1038/s41586-021-04120-y

Punjani, A., J.L. Rubinstein, D.J. Fleet, and M.A. Brubaker. 2017. cryoSPARC: Algorithms for rapid unsupervised cryo-EM structure determination. *Nat. Methods.* 14:290–296. https://doi.org/10.1038/nmeth.4169

Reincke, S.M., M. Yuan, H.C. Kornau, V.M. Corman, S. van Hoof, E. Sanchez-Sendin, M. Ramberger, W. Yu, Y. Hua, H. Tien, et al. 2022. SARS-CoV-2 Beta variant infection elicits potent lineage-specific and cross-reactive antibodies. *Science.* 375:782–787. https://doi.org/10.1126/science.abm5835

Robbiani, D.F., C. Gaebler, F. Muecksch, J.C.C. Lorenzi, Z. Wang, A. Cho, M. Agudelo, C.O. Barnes, A. Gazumyan, S. Finkin, et al. 2020. Convergent antibody responses to SARS-CoV-2 in convalescent individuals. *Nature.* 584:437–442. https://doi.org/10.1038/s41586-020-2456-9

Schmidt, F., Y. Weisblum, F. Muecksch, H.H. Hoffmann, E. Michailidis, J.C.C. Lorenzi, P. Mendoza, M. Rutkowska, E. Bednarski, C. Gaebler, et al. 2020. Measuring SARS-CoV-2 neutralizing antibody activity using pseudotyped and chimeric viruses. *J. Exp. Med.* 217:e20201181. https://doi.org/10.1084/jem.20201181

Schmidt, F., F. Muecksch, Y. Weisblum, J. Da Silva, E. Bednarski, A. Cho, Z. Wang, C. Gaebler, M. Caskey, M.C. Nussenzweig, et al. 2022. Plasma neutralization of the SARS-CoV-2 Omicron variant. *N. Engl. J. Med.* 386:599–601. https://doi.org/10.1056/NEJMc2119641

Schmidt, T., V. Klemis, D. Schub, J. Mihm, F. Hielscher, S. Marx, A. Abu-Omar, L. Ziegler, C. Guckelmus, R. Urschel, et al. 2021. Immunogenicity and reactogenicity of heterologous ChAdOx1 nCoV-19/mRNA vaccination. *Nat. Med.* 27:1530–1535. https://doi.org/10.1038/s41591-021-01464-w

Self, W.H., M.W. Tenforde, J.P. Rhoads, M. Gaglani, A.A. Ginde, D.J. Douin, S.M. Olson, H.K. Talbot, J.D. Casey, N.M. Mohr, et al. 2021. Comparative effectiveness of moderna, pfizer-BioNTech, and janssen (Johnson & Johnson) vaccines in preventing COVID-19 hospitalizations among adults without immunocompromising conditions: United States, march-august 2021. *MMWR Morb. Mortal. Wkly. Rep.* 70:1337–1343. https://doi.org/10.15585/mmwr.mm7038e1

Sievers, F., A. Wilm, D. Dineen, T.J. Gibson, K. Karplus, W. Li, R. Lopez, H. McWilliam, M. Remmert, J. Soding, et al. 2011. Fast, scalable generation of high-quality protein multiple sequence alignments using clustal Omega. *Mol. Syst. Biol.* 7:539. https://doi.org/10.1038/msb.2011.75

Soto, C., R.G. Bombardi, A. Branchizio, N. Kose, P. Matta, A.M. Sevy, R.S. Sinkovits, P. Gilchuk, J.A. Finn, and J.E. Crowe Jr. 2019. High frequency of shared clonotypes in human B cell receptor repertoires. *Nature.* 566:398–402. https://doi.org/10.1038/s41586-019-0934-8

Tortorici, M.A., and D. Veesler. 2019. Chapter four: Structural insights into coronavirus entry. *Adv. Virus Res.* 105:93–116. https://doi.org/10.1016/bs.aivir.2019.08.002

Tortorici, M.A., M. Beltramello, F.A. Lempp, D. Pinto, H.V. Dang, L.E. Rosen, M. McCallum, J. Bowen, A. Minola, S. Jaconi, et al. 2020. Ultrapotent human antibodies protect against SARS-CoV-2 challenge via multiple mechanisms. *Science.* 370:950–957. https://doi.org/10.1126/science.abe3354

Vilches, T.N., S.M. Moghadas, P. Sah, M.C. Fitzpatrick, A. Shoukat, A. Pandey, and A.P. Galvani. 2022. Estimating COVID-19 infections, hospitalizations, and deaths following the US vaccination campaigns during the pandemic. *JAMA Netw. Open.* 5:e2142725. https://doi.org/10.1001/jamanetworkopen.2021.42725

Wang, L., T. Zhou, Y. Zhang, E.S. Yang, C.A. Schramm, W. Shi, A. Pegu, O.K. Oloniniyi, A.R. Henry, S. Darko, et al. 2021a. Ultrapotent antibodies against diverse and highly transmissible SARS-CoV-2 variants. *Science.* 373:eabh1766. https://doi.org/10.1126/science.abh1766

Wang, Z., J.C.C. Lorenzi, F. Muecksch, S. Finkin, C. Viant, C. Gaebler, M. Cipolla, H.H. Hoffmann, T.Y. Oliveira, D.A. Oren, et al. 2021b. Enhanced SARS-CoV-2 neutralization by dimeric IgA. *Sci. Transl. Med.* 13:eabf1555. https://doi.org/10.1126/scitranslmed.abf1555

Wang, Z., F. Muecksch, D. Schaefer-Babajew, S. Finkin, C. Viant, C. Gaebler, H.H. Hoffmann, C.O. Barnes, M. Cipolla, V. Ramos, et al. 2021c. Naturally enhanced neutralizing breadth against SARS-CoV-2 one year after infection. *Nature*. 595:426–431. https://doi.org/10.1038/s41586-021-03696-9

Wang, Z., F. Schmidt, Y. Weisblum, F. Muecksch, C.O. Barnes, S. Finkin, D. Schaefer-Babajew, M. Cipolla, C. Gaebler, J.A. Lieberman, et al. 2021d. mRNA vaccine-elicited antibodies to SARS-CoV-2 and circulating variants. *Nature*. 592:616–622. https://doi.org/10.1038/s41586-021-03324-6

Wang, Z., F. Muecksch, A. Cho, C. Gaebler, H.-H. Hoffmann, V. Ramos, S. Zong, M. Cipolla, B. Johnson, F. Schmidt, et al. 2022a. Conserved neutralizing epitopes on the N-Terminal domain of variant SARS-CoV-2 spike proteins. *bioRxiv*. https://doi.org/10.1101/2022.02.01.478695 (Preprint posted February 1, 2022)

Wang, Z., F. Muecksch, A. Cho, C. Gaebler, H.H. Hoffmann, V. Ramos, S. Zong, M. Cipolla, B. Johnson, F. Schmidt, et al. 2022b. Analysis of memory B cells identifies conserved neutralizing epitopes on the N-terminal domain of variant SARS-Cov-2 spike proteins. *Immunity*. 55:998–1012.e8. https://doi.org/10.1016/j.immuni.2022.04.003

Watanabe, Y., L. Mendonca, E.R. Allen, A. Howe, M. Lee, J.D. Allen, H. Chawla, D. Pulido, F. Donnellan, H. Davies, et al. 2021. Native-like SARS-CoV-2 spike glycoprotein expressed by ChAdOx1 nCoV-19/AZD1222 vaccine. *ACS Cent. Sci.* 7:594–602. https://doi.org/10.1021/acscentsci.1c00080

Weisblum, Y., F. Schmidt, F. Zhang, J. DaSilva, D. Poston, J.C. Lorenzi, F. Muecksch, M. Rutkowska, H.H. Hoffmann, E. Michailidis, et al. 2020. Escape from neutralizing antibodies by SARS-CoV-2 spike protein variants. *Elife*. 9:e61312. https://doi.org/10.7554/eLife.61312

Wu, F., S. Zhao, B. Yu, Y.M. Chen, W. Wang, Z.G. Song, Y. Hu, Z.W. Tao, J.H. Tian, Y.Y. Pei, et al. 2020. A new coronavirus associated with human respiratory disease in China. *Nature*. 579:265–269. https://doi.org/10.1038/s41586-020-2008-3

Yuan, M., H. Liu, N.C. Wu, C.D. Lee, X. Zhu, F. Zhao, D. Huang, W. Yu, Y. Hua, H. Tien, et al. 2020. Structural basis of a shared antibody response to SARS-CoV-2. *Science*. 369:1119–1123. https://doi.org/10.1126/science.abd2321

Zhang, Z., J. Mateus, C.H. Coelho, J.M. Dan, C.R. Moderbacher, R.I. Gálvez, F.H. Cortes, A. Grifoni, A. Tarke, J. Chang, et al. 2022. Humoral and cellular immune memory to four COVID-19 vaccines. *Cell*. 185:2434–2451.e17. https://doi.org/10.1016/j.cell.2022.05.022
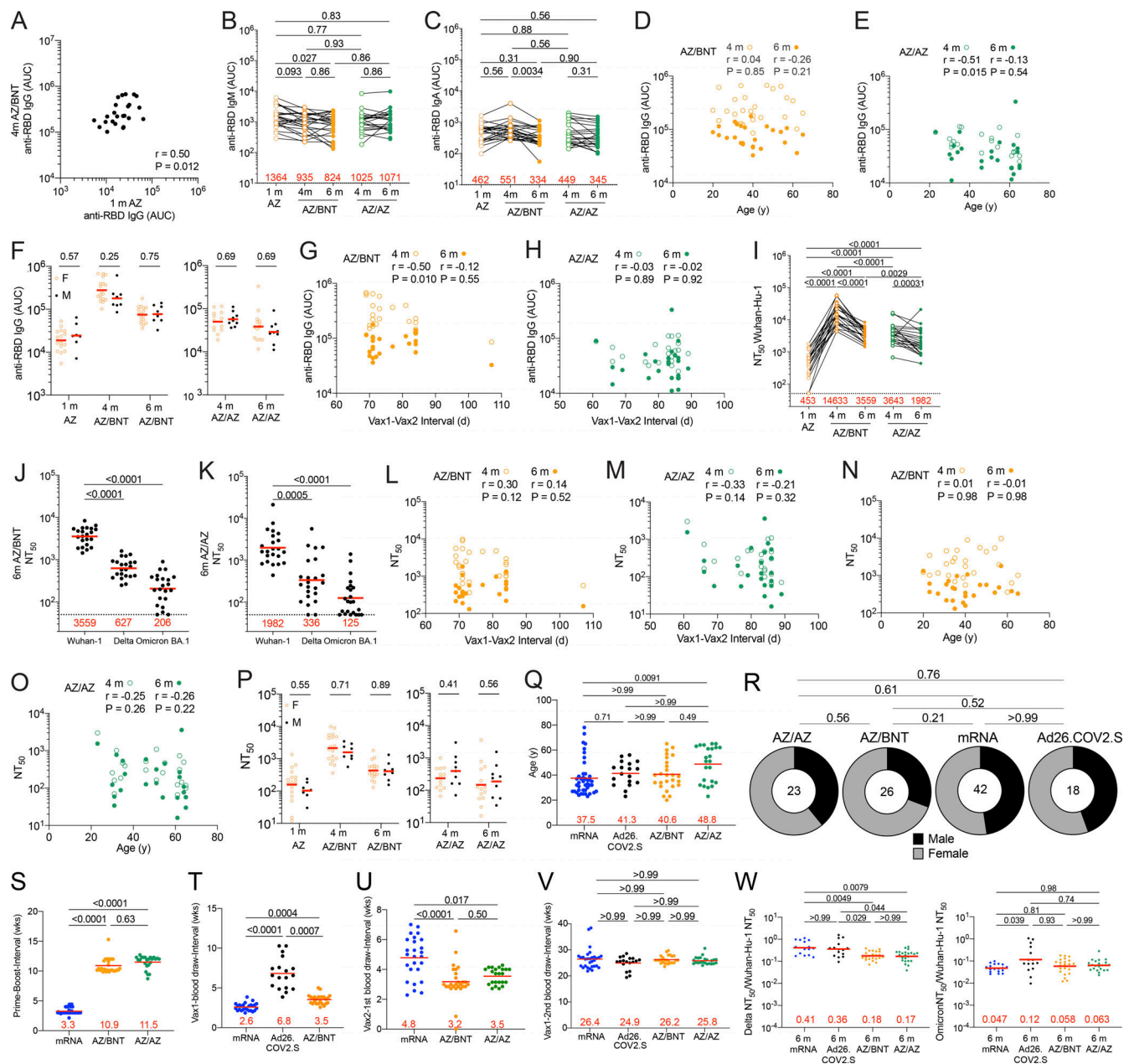
Supplemental material

Figure S1. **Demographics and plasma correlations. (A)** AUC for anti-RBD IgG at 1 mo (m) after ChAdOx1 (AZ) prime plotted against AUC for anti-RBD IgG at 4 mo after initial dose following the ChAdOx1/BNT162b2 AZ/BNT scheme. **(B and C)** AUC for (B) plasma IgM and (C) plasma IgA antibody binding to SARS-CoV-2 Wuhan-Hu-1 RBD 1 mo after AZ prime, as well as 4 and 6 mo after initial dose with either BNT162b2 (AZ/BNT; n = 26) or ChAdOx1 (AZ/AZ; n = 23). Lines connect longitudinal samples. **(D and E)** Age (x axis) plotted against AUC (y axis) for anti-RBD IgG at 4 and 6 mo after initial dose following (D) the AZ/BNT scheme or (E) the AZ/AZ scheme. **(F)** AUC for anti-RBD IgG 1 mo after prime, as well as 4 and 6 mo after initial dose for all male (M; n = 8) or women (F; n = 18) vaccinated following the AZ/BNT scheme (left panel), or AUC for anti-RBD IgG 4 and 6 mo after initial dose for all male (M; n = 9) or female (F; n = 14) following the AZ/AZ scheme (right panel). **(G and H)** Interval between first and second vaccination (x axis) plotted against AUC for anti-RBD IgG (y axis) at 4 and 6 mo after initial dose following (G) the AZ/BNT scheme or (H) the AZ/AZ scheme. **(I–K)** Plasma-neutralizing activity against indicated SARS-CoV-2 variants of interest/concern for n = 45 randomly selected samples assayed in HT1080Ace2 cl.14 cells. Viruses in I–K contained the R683G furin cleavage site mutation to increase particle infectivity (see also Fig. 1, J–M). **(L and M)** Interval between first and second vaccination (x axis) plotted against NT_{50} values (y axis) 4 and 6 mo after initial dose following (L) the AZ/BNT scheme or (M) the AZ/AZ scheme. **(N and O)** Age (x axis) plotted against NT_{50} values (y axis) 4 and 6 mo after initial dose following (N) the AZ/BNT scheme or (O) the AZ/AZ scheme. **(P)** NT_{50} values at 1 mo after AZ prime, as well as 4 and 6 mo after initial dose for all male (M; n = 8) or female (F; n = 18) following the AZ/BNT scheme (left panel), or NT_{50} values at 4 and 6 mo after initial dose for all male (M; n = 9) or female (F; n = 14) following the AZ/AZ scheme (right panel). **(Q–V)** Demographic characteristics. Age (Q), gender (R), and intervals between vaccine doses and blood collections (S–V) are comparable between AZ/AZ and AZ/BNT participants within the AZ cohort. **(W)** Ratio comparison of plasma-neutralizing titers (NT_{50}) against Delta (left panel) or Omicron BA.1 (right panel) to Wuhan-Hu-1 among four vaccine platforms. All experiments were performed at least in duplicate. Red bars represent geometric mean values. r and P values were determined by two-tailed Spearman's correlation (D, E, G, H, and L–O). Statistical significance was determined by two-tailed Mann-Whitney test followed by Holm-Šídák test for multiple comparisons (F, J, K, and P), or by Wilcoxon matched-pairs signed rank test for paired observations followed by Holm-Šídák test for multiple comparisons (B, C, I, Q, and S–W), or a two-tailed Chi-square test (R).
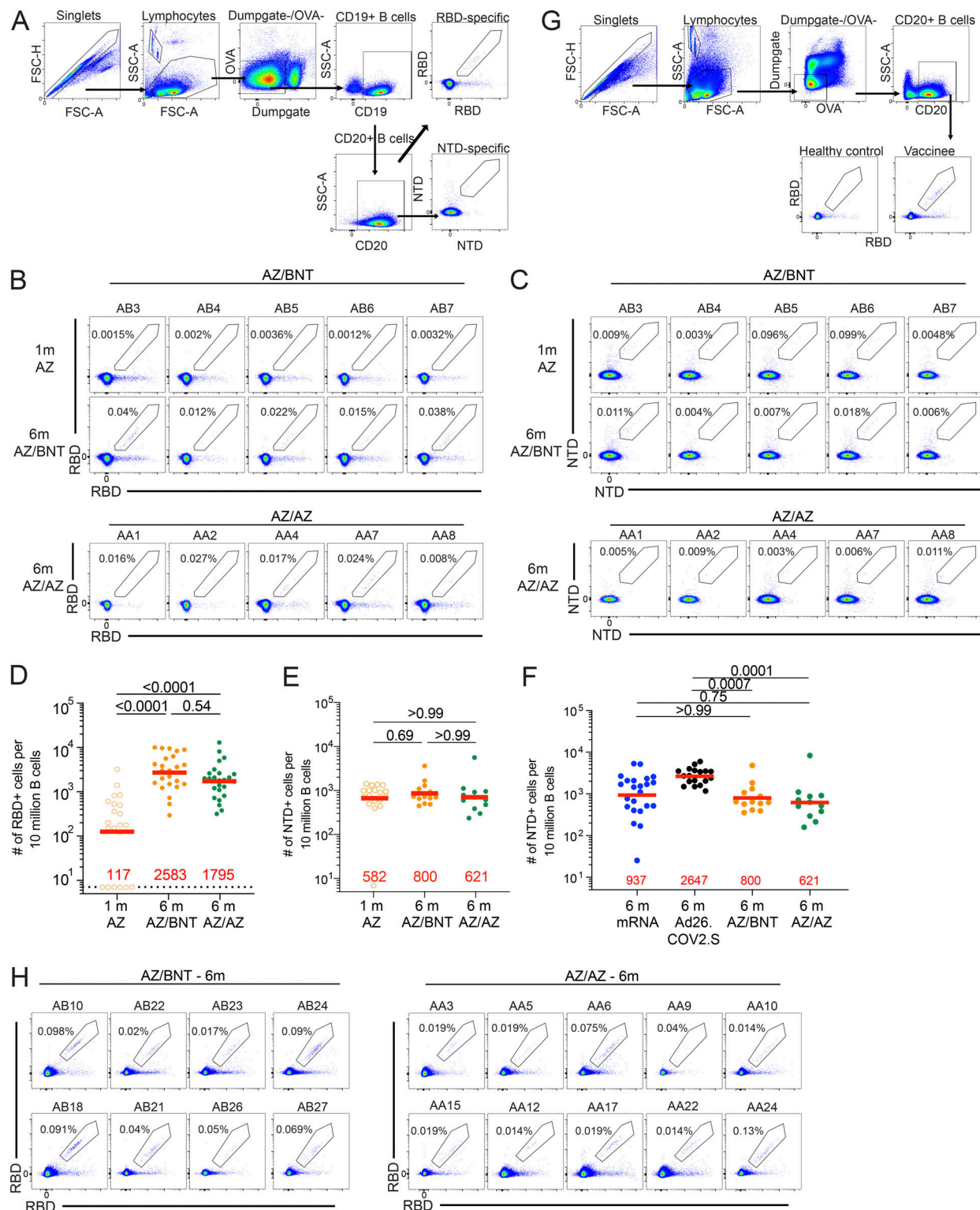
Figure S2. **Flow cytometry. (A)** Gating strategy for phenotyping. Gating was on lymphocytes singlets that were CD19$^+$ or CD20$^+$ and CD3$^-$CD8$^-$CD16$^-$Ova$^-$. Antigen-specific cells were detected based on binding to Wuhan-Hu-1 RBD-PE$^+$ and RBD-AF647$^+$, or to Wuhan-Hu-1 NTD-BrilliantViolet-711$^+$ and NTD-BrilliantViolet-421$^+$. Counting beads were added to each sample and gated based on forward scatter (FSC) and side scatter (SSC) as per manufacturer instructions. **(B and C)** Representative flow cytometry plots of (B) RBD-binding B cells or (C) NTD-binding B cells in five individuals 1 mo (m) after AZ prime and 6 mo after initial dose. **(D–F)** Graph showing the frequency of Wuhan-Hu-1 RBD-specific B cells and NTD-BV711 and NTD-BV421 binding B cells. **(G)** Gating strategy for single-cell sorting for CD20$^+$ B cells for RBD-PE and RBD-AF647. Healthy control was pre-pandemic. **(H)** Representative flow cytometry plots showing dual AlexaFluor-647- and PE-Wuhan-Hu-1-RBD binding, single-cell sorted B cells from AZ/BNT and AZ/AZ vaccinees 6 mo after initial dose. Statistical significance in C–E were determined by two-tailed Kruskal Wallis test with subsequent Dunn's multiple comparisons. All experiments were performed at least in duplicate.
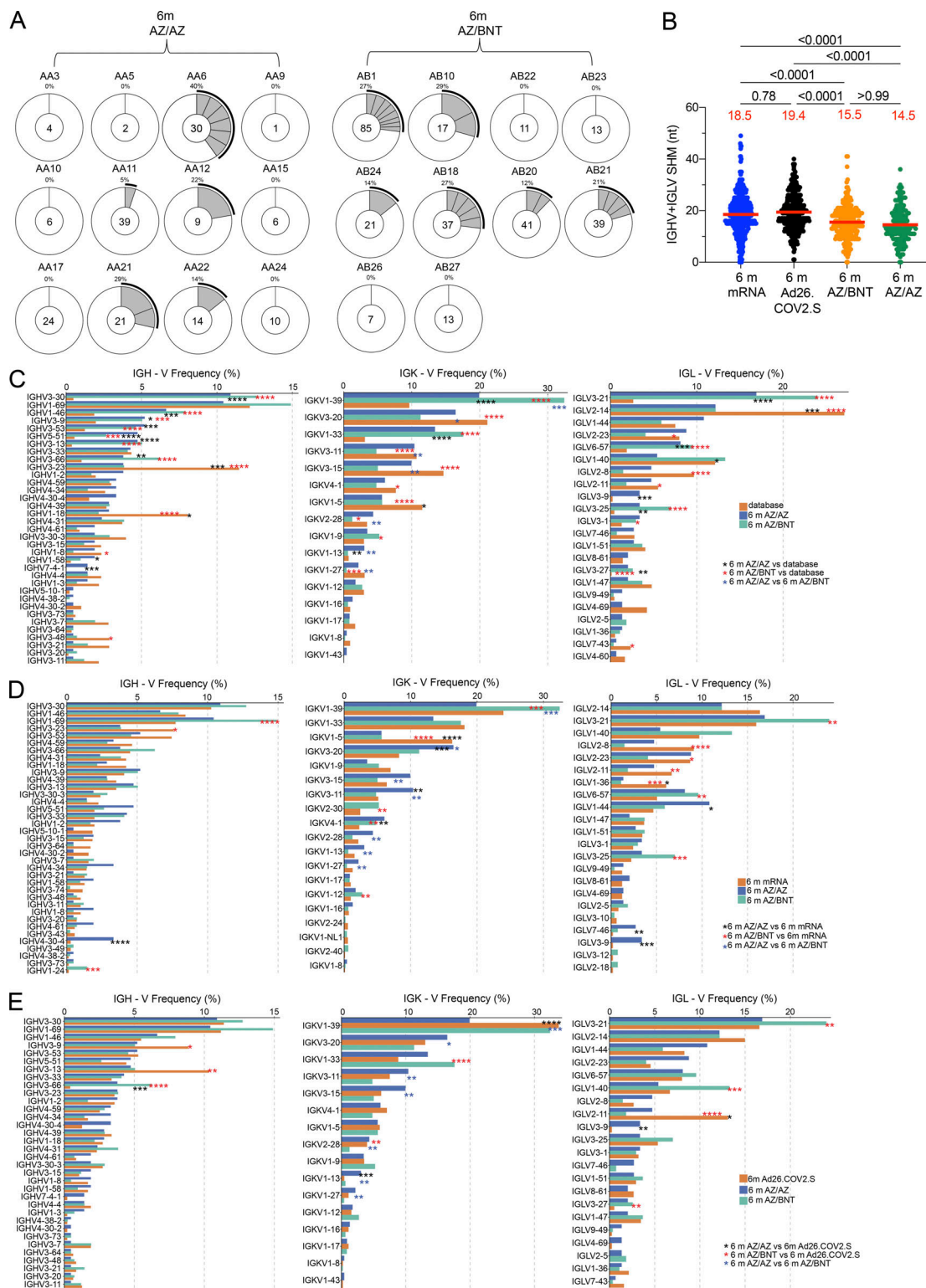
Wang et al.
In-depth immunological COVID-19 vaccine comparison

Journal of Experimental Medicine   S3
https://doi.org/10.1084/jem.20220826

Figure S3. **Clonality and V gene usages of anti–SARS-CoV-2 Wuhan-Hu-1 RBD antibody. (A)** Pie charts show the distribution of IgG antibody sequences obtained from MBCs from Wuhan-Hu-1 RBD-specific memory B cells of AZ/BNT and AZ/AZ vaccinees 6 mo (m) after initial dose. The number inside the circle indicates the number of sequences analyzed for the individual denoted above the circle. **(B)** Same as Fig. 2 E, but showing only one representative member of each expanded antibody clone. **(C–E)** Comparison of the frequency distribution of human V genes for heavy and light chains of anti-RBD Wuhan-Hu-1 antibodies from this study and from a database of shared clonotypes of human B cell receptor generated by Cinque (Soto et al., 2019). Graph shows relative abundance of human IGHV, IGKV and IGLV genes, with 6-mo AZ/AZ antibodies (blue) and AZ/BNT antibodies (green). **(C)** Sequence Read Archive accession SRP010970 (orange). **(D)** Antibodies from mRNA vaccinees 6 mo after initial dose (orange; Cho et al., 2021). **(E)** Antibodies from Ad26.COV.2S vaccinees 6 mo after prime (orange; Cho et al., 2022). Statistical significance was determined by two-tailed Kruskal–Wallis test with subsequent Dunn's multiple comparisons in B and by two-sided binomial test. *, P ≤ 0.05; **, P ≤ 0.01; ***, P ≤ 0.001; ****, P ≤ 0.0001 in C–E.
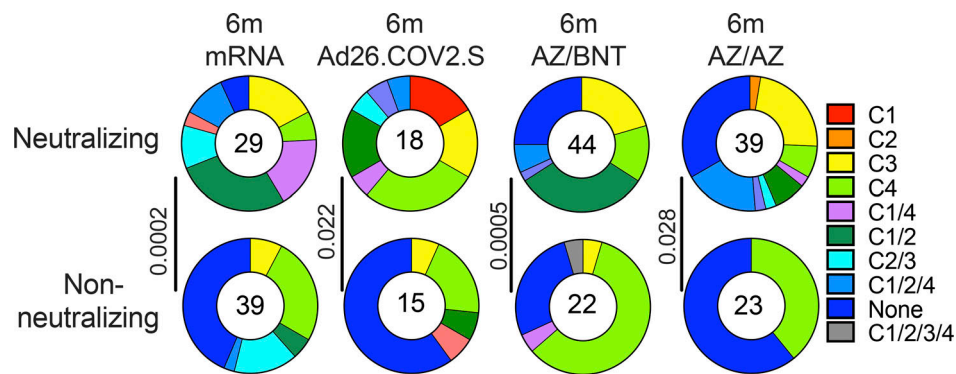
Figure S4. **Epitope mapping.** Results of epitope mapping performed by competition BLI. Pie charts show the distribution of the antibody classes among all neutralizing antibodies against Wuhan-Hu-1 and non-neutralizing antibodies obtained from mRNA vaccinees at 6 mo (m) after initial dose (n = 68; Cho et al., 2021), Ad26.COV.2S vaccinees at 6 mo (n = 33) after prime (Cho et al., 2022), to mAbs cloned from AZ/AZ (n = 62) or AZ/BNT(n = 66) vaccinees 6 mo after initial dose. Pie charts were compared using a two-tailed Fisher's exact test.
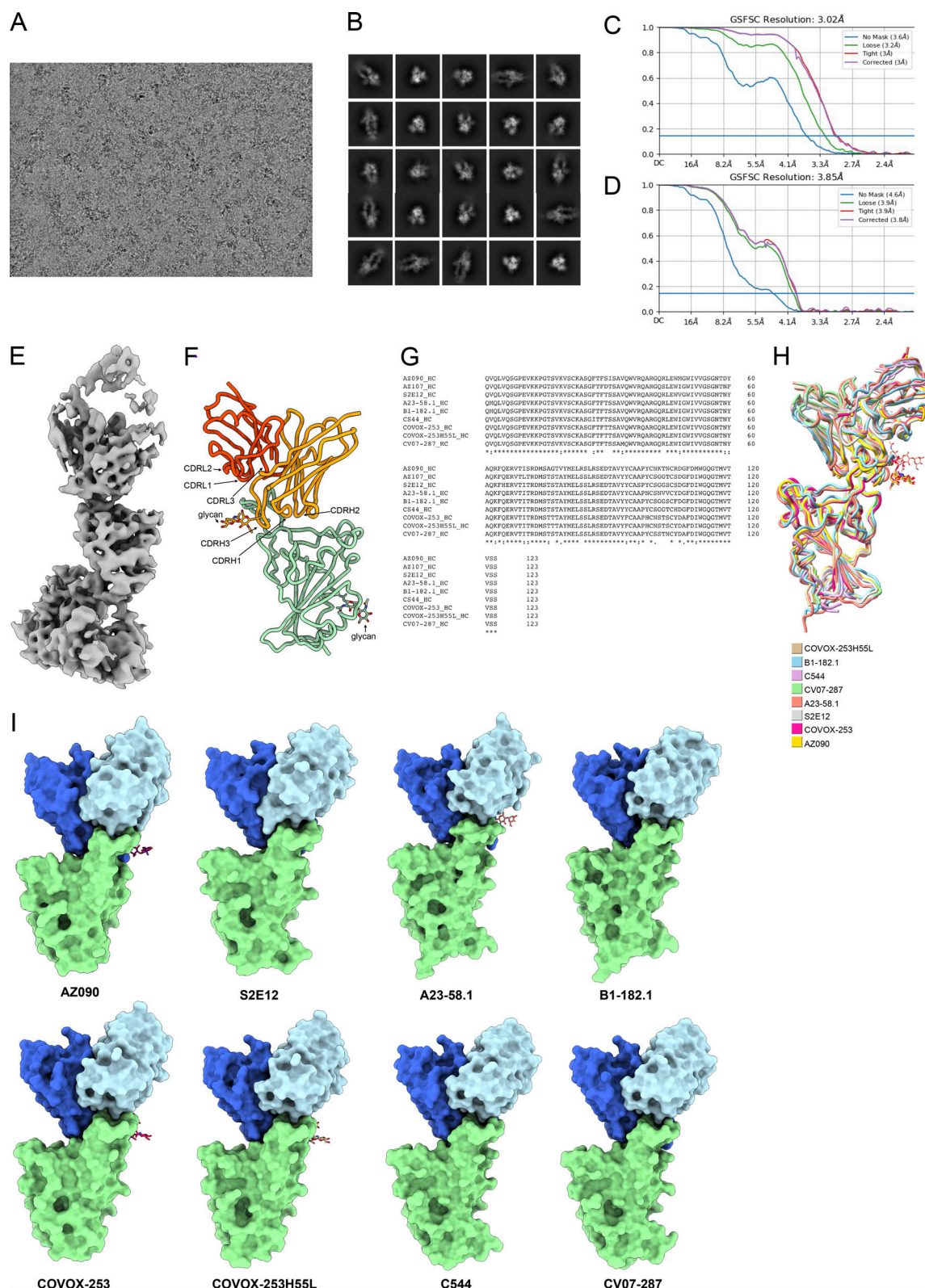
Figure S5. Cryo-EM data processing. (A) Representative cryo-EM micrograph from whole dataset. **(B)** 2D class averages of selected particles for homogeneous refinement. **(C)** Gold-standard Fourier shell correlation curves for the whole map of S 6P bound to AZ090 Fabs. **(D)** Gold-standard Fourier shell correlation curves for the map of the RBD-AZ090 Fab region. **(E)** Cryo-EM density of RBD-AZ090 Fab region. **(F)** Model of Fab fragment bound to RBD of SARS-CoV-2 is shown as cartoon. The glycans are shown as stick. The heavy chain of AZ090 is colored orange, and the light chain of AZ090 is colored orange red. **(G)** Multiple sequence alignment of RBDs was processed by Clustal Omega (Sievers et al., 2011). **(H)** RBD-Fab structures sharing the same usage of heavy chain gene are aligned. Different models are colored respectively. **(I)** Structures from H are shown as cartoon. The RBDs are colored green, the heavy chains are colored royal blue, and the light chains are colored light blue. The glycans on the heavy chains are shown as stick.

Provided online are Table S1, Table S2, Table S3, Table S4, and Table S5. Table S1 details individual characteristics for participants who received AZ/AZ or AZ/BNT vaccines. Table S2 details sequence information of all characterized RBD-binding memory B cells from AZ/AZ or AZ/BNT vaccinated individuals. Table S3 provides information of all recombinant mAbs cloned from RBD-binding B cells. Table S4 provides information of neutralization breath against a panel of variants that tested on selected number of recombinant mAbs. Table S5 provides parameters for cryo-EM.